Water mass circulation and residence time using Eulerian approach in a large coastal lagoon (Nokoué Lagoon, Benin, West Africa)

Kodjo Jules Honfo, Alexis Chaigneau, Yves Morel, Thomas Duhaut, Patrick Marsaleix, Olaègbè Victor Okpeitcha, Thomas Stieglitz, Sylvain Ouillon, Ezinvi Baloitcha, Fabien Rétif

Water mass circulation and residence time using Eulerian approach in a large coastal lagoon (Nokoué Lagoon, Benin, West Africa).

Kodjo Jules Honfo [abc*], Alexis Chaigneau [abc], Yves Morel [agf], Thomas Duhaut [a], Patrick Marsaleix [a], Olaègbè Victor Okpeitcha [bcd], Thomas Stieglitz [e], Sylvain Ouillon [a], Ezinvi Baloitcha [c], Fabien Rétif [f]

[a] Laboratoire d'Études en Géophysique et Océanographie Spatiale (LEGOS), Université de Toulouse, CNES, CNRS, IRD, UPS, Toulouse, France,

[b] Institut de Recherches Halieutiques et Océanologiques du Bénin (IRHOB), Cotonou, Benin,

[c] International Chair in Mathematical Physics and Applications (ICMPA–UNESCO Chair), University d'Abomey-Calavi, Cotonou, Benin

[d] Laboratoire d'Hydrologie Appliquée (LHA), Institut National de l'Eau (INE), African Centre of Excellence for Water and Sanitation (C2EA), Université d'Abomey Calavi, Bénin

[e] Aix-Marseille Université, CNRS, IRD, INRAE, Coll France, CEREGE, Aix-en-Provence, France

[f] SNALE, Aubenas, France

[g] Laboratoire d'Océanographie Physique et Spatiale (LOPS), Université de Brest, CNRS, IRD, Ifremer, IUEM, Brest, France

Corresponding author: honfojules9@gmail.com

Abstract

Seasonal water circulation and residence times in the large (150 km^2) and shallow (1.3 m average dry season depth) Nokoué Lagoon (Benin) are analyzed by means of numerical simulations using the three-dimensional SYMPHONIE model. The average circulation during the four primary hydrological periods throughout the year are studied in detail. Despite the lagoon's shallowness, significant disparities between surface and bottom conditions are observed. During the flood season (September-November), substantial river inflow (~1200 m^3/s) leads to nearly barotropic currents (~7 cm/s), 'directly' linking rivers to the Atlantic Ocean. Rapid flushing results in short water residence times ranging from 3 to 16 days, with freshwater inflow and winds driving lagoon dynamics. During the salinization period (December-January) the circulation transforms into an estuarine pattern, characterized by surface water exiting and oceanic water entering the lagoon at the bottom. Average currents (~2 cm/s) and recirculation cells are relatively weak, resulting in a prolonged residence time of approximately 4 months. Circulation during this time is dominated by tides, the ocean-lagoon salinity gradient, wind, and river discharge (~100 m^3/s). During low-water months (February to June), minimal river inflow and low lagoon water-levels prevail. Predominant southwest winds generate a small-scale circulation (~3 cm/s) with a complex pattern of multiple recirculation and retention cells. Residence times vary from 1 to 4 months, declining from February to June. During the lagoon's desalination season (July-August), increasing river inflows again establish a direct river-ocean connection, and average residence times reduce to ~20 days. Notably, a critical river discharge threshold (~50-100 m^3/s) is identified, beyond which the lagoon empties within days. This study highlights how wind-driven circulation between December and June can trap water along with potential pollutants, while river inflows, tides, and the ocean-lagoon salinity gradient facilitate water discharge. Additionally, it explores the differences between residence and flushing times, as well as some of the limitations identified in the simulations used.

Keywords: Lagoon Circulation; Residence time; Nokoué Lagoon; Numerical modelling; Forcings;

1. Introduction

Coastal lagoons account for approximately 13% of the world's coastal zones (Kjerfve, 1994). They play a crucial role as transition zones between land and ocean, marked by significant spatio-temporal variations in physical, biogeochemical, and ecological parameters (Pérez-Ruzafa et al., 2019; Du et al., 2019; Torres et al., 2020). Lagoons provide a wide range of ecosystem services, supporting flood prevention, food production, biodiversity preservation, and economic activities such as fishing, tourism, aquaculture, sand extraction, transportation, and more (Newton et al., 2018). Although they are often protected as wetlands, lagoons remain vulnerable to pressures related to climate change and human activities.

A thorough understanding of water mass circulation and residence time within lagoons is essential to assess the environmental and ecological consequences of their exploitation. The intricacies of water movements influence the dispersion of nutrients, contaminants, and other substances, with notable impacts on water quality and ecosystem well-being (Mohanty, 2009; Lane et al., 2011; Béjaoui et al., 2016). The water residence time, in turn, allows for the assessment of nutrient and pollutant retention within the lagoons, as well as their potential concentration or degradation. Furthermore, water circulation and residence times have the potential to shape habitats for lagoon-dwelling flora and fauna, as well as the economic activities that depend on them (Balotro, 2003; Sylaios et al., 2006; Ferrarin et al., 2013; Panda et al., 2015).

Coastal lagoons are subject to a variety of physical forcings that influence their dynamics and the residence times of water masses. These physical drivers include freshwater inflow from catchments, the intrusion and propagation of ocean tide through inlets, wind effects, or evaporation-precipitation fluxes (Balotro, 2003; Lovato, 2010; O'Callaghan, 2011; Morales, 2020). Across various frequencies, including semi-diurnal, diurnal, and fortnightly cycles, tides can lead to fluctuations in water levels and alternating currents between the lagoon and the ocean (Sylaios et al., 2003; O'Callaghan et al, 2007). These ocean-lagoon exchanges are typically accompanied by residual currents resulting from non-linear interactions between tidal flow and local topography. These currents are important in the dispersion of salt or phytoplankton, the transport of pollutants and the generation of turbidity maxima (Maier-Reimier, 1977; Robinson 1981; Sylaios et al., 2003; O'Callaghan et al., 2007; Du et al., 2019). Furthermore, the seasonal variation in freshwater inflows associated with precipitation and river flow regimes can impact lagoon dynamics in two key ways: i) by diluting the saltwater from the ocean and the resulting density gradient that drives gravitational circulation, and ii) by creating, at seasonal scales, river-inlet connections contributing to the flushing process (Pritchard, 1952; Lerczak and Geyer, 2006; O'Callaghan et al., 2007; Sassi, 2013). Semi-permanent seasonal winds give rise to intricate circulation patterns, contingent upon factors such as basin shape, wind direction, the vertical extent of turbulence, and variations in basin bathymetry (Geyer, 1997; Lovato, 2010; O'Callaghan, 2011). These combined

processes collectively influence lagoon dynamics, the distribution and dispersion of water masses, nutrients and pollutants, as well as the residence times of these substances within the lagoon.

In West Africa, the coastal zone along the Gulf of Guinea is characterized by a series of coastal lagoons (Allersma and Tilmans, 1993; Adite and Winemiller, 1997; Lalèyè et al., 2007; Adite et al, 2013) that provide essential ecosystem services to local communities (Pérez-Ruzafa et al., 2011; Djihouessi et al., 2017; Newton et al., 2018). Additionally, these lagoons serve as sanctuaries, feeding grounds, breeding sites, and nurseries for a diverse array of aquatic species (Pérez-Ruzafa et al., 2011; Djihouessi et al., 2017; Panda et al., 2015; Newton et al., 2018). Among West African lagoons, Nokoué Lagoon, located in southeastern Benin (Fig. 1), stands out as one of the most biologically productive in the region (Lalèyè et al., 1995, 2003, 2007).

The Nokoué Lagoon, housing the largest lacustrine villages in West Africa, is subject to significant natural variability, characterized by major seasonal changes in its physico-chemical parameters driven by the hydrological regime (e.g. Djihouessi and Aina, 2018). Notably, the lagoon's salinity exhibits significant seasonal fluctuations (Okpeitcha et al., 2022), leading to considerable alterations in the composition and abundance of its ecosystem, ranging from plankton (Chaigneau et al., 2023) to fish (Lalèyè et al., 2003). Recent studies, based on an intensive observational monitoring network unique in the region and the development of simplified models, have contributed to a better understanding and description of the Nokoué Lagoon's functioning (e.g. Okpeitcha et al., 2022; Chaigneau et al., 2022; 2023; Morel et al., 2022). However, the intricate water mass circulation, crucial for the redistribution of physico-chemical properties and larval transport (Avigdor and Mark, 1997; Mohanty, 2009), remains undocumented due to the challenges of obtaining observational data in this shallow and exploited environment. The aim of our study is to address this gap using realistic three-dimensional numerical simulations.

Due to urban development and strong population growth in the study region, the Nokoué Lagoon faces substantial anthropogenic pressure (Dovonou et al, 2011; Zandagba et al. 2016), evident in elevated levels of pollutants including heavy metals, pesticides and fecal bacteria (Lalèyè et al., 1997; Ogutu - Ohwayo et *al*. 1997; Aina et al., 2012a; 2012b; Adjahouinou et al., 2012, 2014; Yehouenou, 2013). The fate of these pollutants, which are notably associated with wastewater discharge or rainwater runoff from the shores, remains a major concern, given that their concentrations are prone to being elevated in specific locations. This situation mirrors that of other lagoons influenced by reduced freshwater inflow or substantial water retention (Swift and Bower, 2003; Sale et al., 2011; Baohong et al., 2013; Lucinde et al., 2020; Peng et al., 2021). Hence, our study also aims to document water residence times in Nokoué Lagoon on seasonal scales in order to better understand the fate of these pollutants. Ultimately, through a series of numerical simulations, the final goal of this research is to examine the responsiveness of circulation and residence times to tidal influences, wind patterns, and the salinity gradient existing between the ocean and the lagoon.

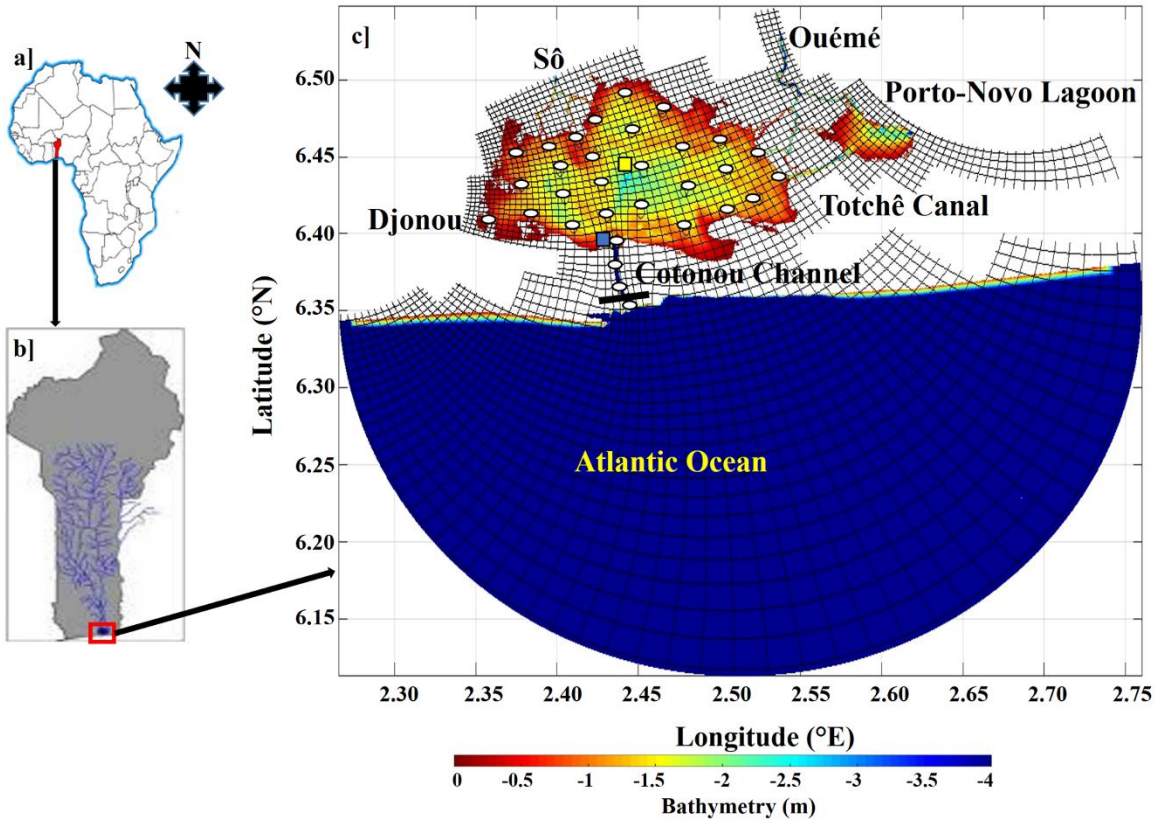

Figure 1: Location of the Nokoué Lagoon: a] Benin in West Africa; b] Nokoué Lagoon and its watershed; c] Bathymetry, measuring stations and model domain. The white circles show the positions of the 31 CTD stations, the blue and yellow squares represent the water level and temperature stations respectively, and the black line is the ADCP section where lagoon-ocean water exchange are measured. The model grid shown is 1 point out of 10.

2. Materials and methods

2.1. Characteristics of the study area

Located in southeastern Benin, Nokoué Lagoon stretches approximately 20 km from east to west and 11 km from south to north, covering an area of around 150 km^2 and maintaining an average depth of 1.3 m during low water, which increases to approximately 2.5 m during the flood season (Texier et al., 1980; Mama et al., 2011; Djihouessi et al., 2019; Chaigneau et al., 2022). The climate is sub-equatorial defined by two alternating rainy periods (May to mid-July and September to October) and two dry seasons (November to April and mid-July to August). On an annual scale, the prevailing winds are characterized by southwesterly monsoon winds (Guèdjè et al., 2019), maintaining a relatively modest average speed of approximately 3 m/s. These winds emanate from the retroflection of the trade winds.

From December to February, *harmattan* wind events originating from the northeast and typically lasting for a few days can occur, with average intensities of around 2 m/s (Guèdjè et al., 2019).

Nokoué Lagoon is fed by two principal rivers, the Ouémé and the Sô (Fig. 1c), flowing into the northern part of the lagoon. Their catchment areas are approximately 50000 km^2 and 1000 km^2 respectively (Mama et al., 2011; Djihouessi et al., 2017). Cumulative river flow is in the range of a few tens of m^3/s during the low-water period (December-July) and peak at around 1200 m^3/s during the flood peak (September-November). This surge in flow and its interaction with tides cause the average lagoon level to rise by approximately 0.9 m between the two seasons (Chaigneau et al., 2022; Morel et al., 2022). A third river, the Djonou, contributes a minor amount of freshwater to the southwestern part of the lagoon, although its flow is negligible compared to that of the Sô and Ouémé rivers (Djihouessi and Aina, 2018). In its southern part, Nokoué Lagoon is connected with the Atlantic Ocean through the Cotonou channel, measuring approximately 300 m in width and 4 km in length (Texier et al., 1980). This channel facilitates the exchange of fresh and saltwater. Consequently, the average salinity of the lagoon fluctuates from near 0 during high-water periods to approximately 25 during low-water periods. Even slight changes in river flow can result in significant shifts in lagoon salinity during these low-water periods (Okpeitcha et al., 2022, 2024). Towards the east, via the 4 km-long Totché canal, Nokoué Lagoon is connected to Porto-Novo Lagoon. This link extends further eastward through a narrow coastal canal that eventually flows into the Atlantic Ocean near Lagos, Nigeria, located about 100 km away (Texier et al., 1980).

2.2. SYMPHONIE model and configuration

The three-dimensional SYMPHONIE free-surface model is used in this study. This model, widely used for coastal ocean modelling (e.g. Estournel et al., 2001; 2005; 2012; Auclair et al., 2001; Marine et al., 2008, 2013; Ulses et al., 2008; Hu et al, 2009; Bouchette et al., 2010; Michaud et al., 2012; Herbert et al., 2011; Onguéné, 2015; Loisel et al., 2017; Nguyen-Duy et al., 2021), is based on the discretized primitive equations on a curvilinear bipolar "Arakawa C" grid (Arakawa and Lamb, 1977) using the finite difference and energy conservation method (Marsaleix et al., 2006; 2008). The k-epsilon turbulent closure scheme, including the wave current effect, was implemented according to Costa et al. (2017). The configuration used for this study encompasses the open ocean, Cotonou channel, Nokoué Lagoon, rivers (So, Ouémé and Djonou) and Porto-Novo lagoon, which closes off towards Nigeria. The horizontal grid features dimensions of 563×646 points, complemented by 10 generalized sigma vertical levels. Mesh size varies from 30 m within the lagoon to 200 m offshore, with finer resolution in the channel and coarser resolution in the open ocean (Fig. 1c). The turbulent closure scheme, important for the vertical redistribution of tracers and momentum, is following the k-epsilon turbulent scheme (Michaud et al., 2012). Bottom friction is taken into account using the logarithmic profile approach and the definition of a roughness parameter Z_0 (Blumberg and Mellor, 1987). For the

results presented below we chose a typical value for the muddy bottom condition in the lagoon with $Z_0 = 5.10^{-4}$ m (see also below and discussion in section 4.2).

The forcings used in the reference simulation are, on one hand, large-scale three-dimensional ocean forcings (temperature, salinity, free surface elevation, currents) from the MERCARTOR system based on the NEMO model (Maraldi et al., 2013). Additionally, tidal forcing is applied from the FES2014 Tidal Atlas, considering the 9 main harmonic components within the domain (M2, N2, S2, K2, K1, O1, P1, Q1 and M4). The astronomical tidal potential was implemented in the moment equations (Pairaud et al., 2008).

On the other hand, atmospheric forcings at the air/sea interface (radiative fluxes, heat fluxes, wind shear stresses) are calculated, in the SYMPHONIE model, from bulk formulae using three-hourly fields from the ECMWF meteorological model (Seyfried et al., 2017).

Finally, the river discharge used to force the model is estimated during flood periods from observed water level differences between the lagoon and the ocean, using an inverse method developed by Morel et al. (2022). Fluxes during low water periods are more challenging to estimate and required calibration through sensitivity analyses. A minimum flux of 7.5 m^3/s was necessary to realistically simulate lagoon desalination near the rivers and reproduce the observed spatio-temporal distribution of salinity at seasonal scales (Okpeitcha et al., 2022; 2024). Salinity serves as a key tracer for the ecosystem, and the accurate modeling of its variability (Okpeitcha et al., 2024) suggests that the seasonal exchanges of water between the watersheds and ocean, as well as the seasonal lagoon circulation and residence times, are realistically represented. The recalibrated river discharges are introduced through the lateral conservation conditions of volume and salinity.

The SYMPHONIE model operates in "splitting mode" with a barotropic time step of ~3 s (external mode) and a baroclinic time step of ~28 s (internal mode). A period of two years was modelled (October 2016 to December 2018), with the initial year (October 2016 – October 2017) considered the model's spin-up. Consequently, this study focuses on analyzing the 15 months of simulation (October 2017 - December 2018), which constitutes the reference simulation labeled as *Ref*.

In order to explore the influence of key driving factors on the circulation and residence times within Nokoué Lagoon, three additional simulations were performed alongside the reference simulation (*Ref*):

- *NoTide* Simulation (*NoTide*): This simulation was run without tidal forcing, omitting the influence of tides on the system.
- *NoSal* Simulation (*NoSal*): In this scenario, the dependence on salinity gradients was removed. Salinity no longer impacts the density equation of state, altering its influence on the system.

- *NoWind* Simulation (*NoWind*): This simulation involved the exclusion of wind forcing from the moment equations, while retaining its significance for mixing assessment.

The primary objective of these simulations was to assess how these key driving factors impact the dynamics of the lagoon. All other external forces and parameters remained identical to the *Ref* simulation. Model outputs were stored at high frequency of approximately 30 minutes and were subsequently used to compute monthly or seasonal averages. Note that these simulations were also used by Okpeitcha et al. (2024) to study the mechanisms involved in the seasonal variations of the salinity in Nokoué Lagoon.

2.3. In-situ data

Between December 2017 and December 2018, 13 monthly multidisciplinary observation campaigns were carried out within the lagoon. These campaigns involved the collection of diverse physico-chemical parameters across 31 uniformly distributed stations positioned throughout the lagoon (see Fig. 1c, white circles). The focus here is on the vertical salinity profiles obtained at these stations through the use of a Conductivity Temperature Depth (CTD) probe (Valeport MIDAS CTD+ 300). The CTD probe operated at a frequency of 8 Hz, capturing data at intervals of approximately 0.1 dbar (equivalent to around 10 cm) across the water column, ranging from the water's surface to the lagoon bottom. Depth at the stations varied between approximately 0.5 meters and 2.5 meters in low water period, as illustrated in Fig. 1c. For each of the 12 monthly surveys, salinity data from the 31 stations were spatially interpolated onto a regular grid of resolution ~100 m × 100 m, using an objective interpolation scheme (Bretherton et al., 1976; McIntosh, 1990; Wong et al., 2003).

Water exchanges between the Atlantic Ocean and the lagoon were assessed at the Cotonou channel through monthly measurements spanning December 2017 to October 2018 using an acoustic Doppler current profiler (ADCP Teledyne RDI WorkHorse 1200-kHz). Installed on a motorized vessel, this instrument captured vertical current profiles at intervals of 1 second along a nominal section oriented transversely to the channel's banks (black line in Fig. 1c). During each monthly campaign, the section was run repeatedly for more than 13 hours, to cover an entire semi-diurnal tidal cycle (which is the main tidal component along the Benin coast). For each of these sections, completed in less than 5 minutes, integration of the currents between the two banks of the channel is used to determine the inflow and outflow through the section. These flow values obtained for each individual section were subsequently averaged over time (~13 hours) to derive an average flow (with a ±1 standard deviation range) between the lagoon and the ocean. This averaging process served to mitigate the influence of semi-diurnal tidal fluctuations. However, the duration of these monthly ADCP campaigns is not sufficient to resolve the

longer tide components such as the diurnal components, which is significant too. Thus, the determined variability, based on semi-diurnal components only, is likely slightly underestimated in the observations.

To monitor fluctuations in water levels within the lagoon, we established a station located in the southern region (blue square in Fig. 1c). This station was equipped with a pressure sensor (Onset HOBO U20L-01 WL) positioned 20-30 cm above the bottom. The sensor was enclosed within a perforated PVC tube with an external diameter of 7 cm. Data collection was conducted continuously at 20-minute intervals from February 2018 to January 2020. The measurements offer a typical accuracy of ±1 cm, with a maximum error of 2 cm (Wilson et al., 2016; Guragai et al., 2018; Chaigneau et al., 2022). Additionally, in the central area of the lagoon, a station was established for the purpose of high-frequency temperature recording (yellow square in Fig. 1c). Near-surface temperature readings were acquired every 30 minutes spanning the period from February 2018 to January 2020.

2.4. Residence times of water in the lagoon

Multiple definitions and methodologies exist for estimating relevant time scales crucial for assessing a lagoon's inherent ability to renew its water masses (Bolin and Rodhe, 1973; Takeoka, 1984; Zimmerman, 1988; Monsen et al., 2002; Abdelrhman, 2002). These time scales can be either global, offering representation for the lagoon as a whole, or local, spatially resolved across lagoon. These estimates can be derived using either Lagrangian or Eulerian approaches (Monsen et al., 2002; Cucco et al, 2009).

In this study, a local residence time (T_R) is computed using a Eulerian approach (e.g. Cucco and Umgiesser, 2006; 2009). This metric is established at every grid point (x,y) of the model, and pertains to the duration required for the concentration of a passive and conservatively dissolved substance ($C(x,y,t)$) -initially introduced into the current field with a concentration $C_0(x,y)$- to significantly decrease. Under the hypothesis of exponential decay (as in Delhez et al., 2004; 2014; Mudge et al, 2008; Cucco et al., 2009; Liu et al., 2010; Umgiesser et al., 2014; Peng et al., 2021), the formulation is represented as:

$$C(x,y,t) = C_0(x,y)e^{-\alpha t} \quad (5)$$

Consequently, T_R is defined by $T_R = \frac{1}{\alpha}$, signifying the time necessary for the initial concentration of the conservative substance to decrease by an exponential factor.

Subsequently, the local residence time will be estimated for different time periods by homogeneously seeding the lagoon with a tracer of arbitrary concentration ($C_0(x,y) = 1$) at the start of each period. These introductions of tracer occur every 15 days between October 2017 and October 2018. For each seeding event, the progression of the tracer's concentration is tracked for over 6 months. This comprehensive monitoring facilitates the construction of maps ($T_R(x,y)$) illustrating the spatial distribution of Eulerian residence times.

3. Results

3.1. Model validation

The aim of this Section is to validate the reference simulation (*Ref*) by comparing it with in-situ data encompassing flows within the Cotonou channel, as well as measurements of water level, temperature, and salinity within the Nokoué Lagoon.

a- Flows within the Cotonou channel

Fig. 2 shows the time series of channel-average flow modelled by the *Ref* simulation within the Cotonou channel, juxtaposed with the ADCP measurements during the 11 field campaigns. The simulated flows show strong daily variability around the mean flow, during both low-water periods (~30 ± 1000 m^3/s) and flood periods (~1200 ± 800 m^3/s). Average daily flows aligns relatively well to the river flows forcing the model, yet they exhibit notable variability. This variability occurs across (semi-) diurnal time scales as well as at approximately 14-day intervals, originating from the interplay between ocean tides and river flows (e.g. Morel et al., 2022). The modelled mean flows approximate the observed mean flows, although the variability attributed to tidal signals, observed during the campaigns (± 300-400 m^3/s), is somewhat lower than the simulated daily variability. It is worth noting that these discrepancies in variability might partially stem from the ADCP's flow sampling, which covers only a portion of the day and cannot replicate the diurnal modulation of the semi-diurnal tide. Metrics such as the correlation coefficient, mean difference, normalized mean square error, and ratio of standard deviations between the two datasets are calculated at 0.84, 26 m^3/s, 58%, and 0.71, respectively. The possible impact of stronger tidal currents in the model on our results is further discussed in Section 4.

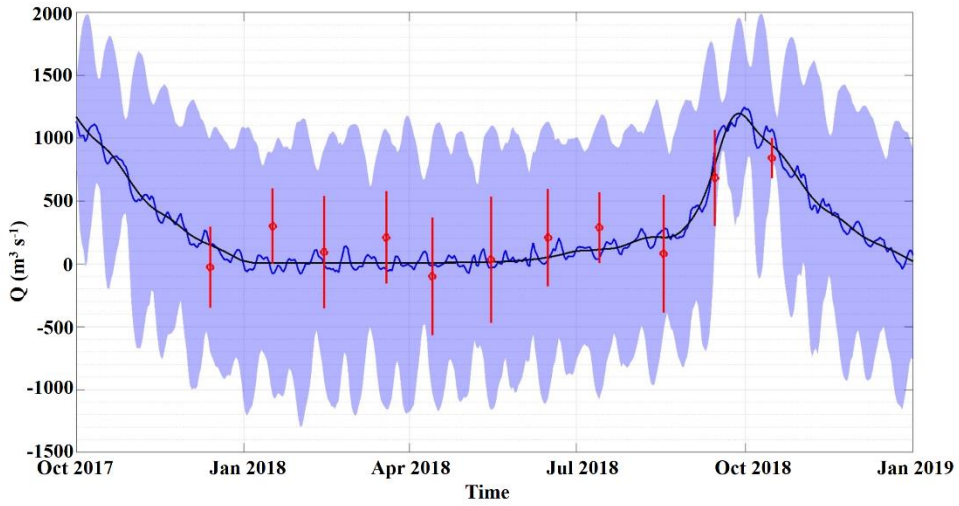

Figure 2: Temporal variation in Cotonou channel flows and total river discharges. The blue curve and shaded area represent the daily mean ± 1 standard deviation of modeled flows. The red circles and vertical bars represent the mean ± 1 standard deviation of observed flows for each of the 11 ADCP campaigns. The black curve represents the total river inflow used to force the numerical simulation. A positive flow corresponds to a net outflow from Nokoué Lagoon to the Atlantic Ocean, while a negative flow corresponds to a net inflow from the ocean into the lagoon.

b- Water level in the lagoon

Fig. 3 shows the time series of observed and modelled water levels in the south of the lagoon. The observations show multi-frequency variations, ranging from a few hours (e.g., seiches or semi-diurnal tides) to seasonal scales, as previously outlined (Chaigneau et al., 2022). Notably, these observations showcase consistent fortnightly water level oscillations, generated by nonlinear interactions involving oceanic spring and neap tides coupled with river dynamics (Morel et al., 2022). Additionally, there is a seasonal surge of approximately 80 cm observed at the peak of flooding in October. These mechanisms are accurately mirrored by the model, although the modeled elevation during peak flooding is slightly lower than observed. The divergence in mean elevation during the flood season between the model and observations might be attributed to several factors, such as the lack of dissipation in the channel during this time of the year (possibly due to structures like bridge piers that generate hydraulic surges not considered by the model). It is also plausible that the river flows forcing the model might not be sufficient during flood periods to attain the observed water level. However, it is worth noting that during this period, we will later demonstrate that the lagoon's rapid flushing results in minimal water retention. Hence, even if the modeled water level exhibits a lower peak elevation during flooding, it does not significantly impact the estimates of residence and flushing times for this season.

The correlation coefficient, mean difference, standardized mean square error, and ratio of standard deviations between the two timeseries are of 0.94, 8 mm, 14% and 0.89, respectively.

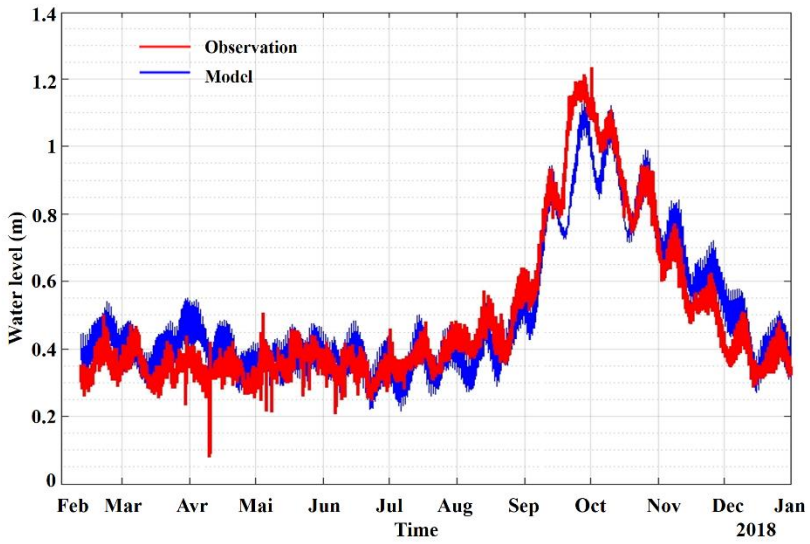

Figure 3: Time series of observed (red line) and modelled (blue line) water levels south of the lagoon.

c- Temperature at the center of the lagoon

Fig. 4 shows temperature variations at the center of Nokoué Lagoon. Measured and modelled temperatures compare well, even though the model slightly overestimates high-frequency tidal variations. Temperatures span from a minimum of 27-29°C during the period between mid-June and mid-September to a peak of 30-31°C from November to May (Fig. 4). The correlation coefficient, mean difference, normalized mean square error, and ratio of standard deviations between the two time series are 0.89, 0.25°C, 2%, and 0.84, respectively. By filtering out the high-frequency tide-induced variations, the low-frequency fluctuations exhibit an improved correlation with a correlation coefficient, mean difference, normalized mean square error, and ratio of standard deviations reaching 0.96, 0.25°C, 1%, and 0.87. These statistical measures affirm the model's adeptness in replicating the observed temporal temperature dynamics.

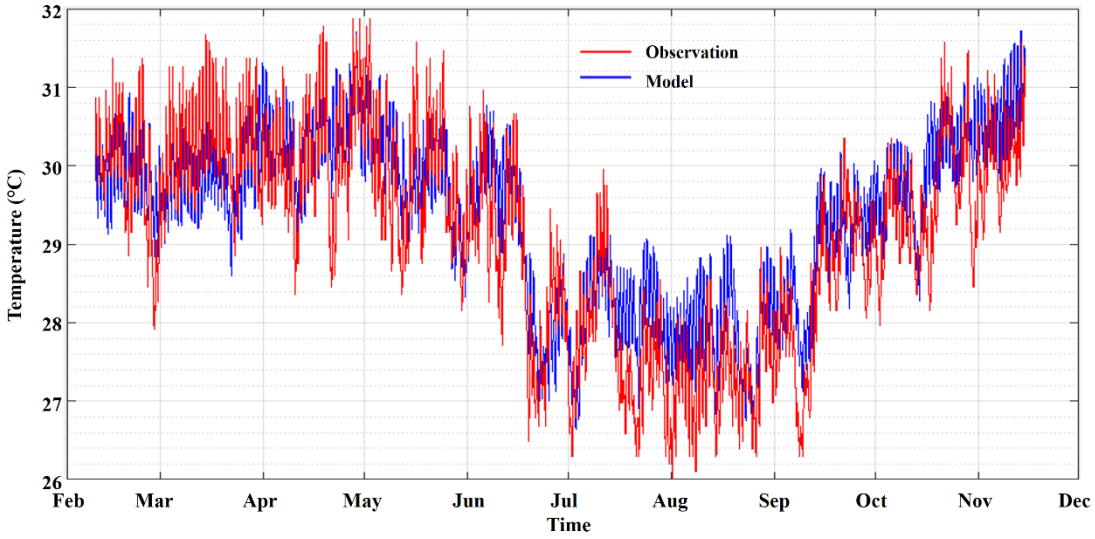

Figure (4): Temporal evolution of observed (red) and modeled (blue) temperature at the center of Nokoué Lagoon between February and December 2018.

d. Salinity in the lagoon

The model also captures well the observed spatial distribution of salinity, particularly evident in March when the lagoon exhibits higher salinity levels (Fig 5a). The correlation coefficient, mean difference, normalized root mean square error, and ratio of standard deviations between the model and observations are approximately 0.70, 0.14 psu, 12%, and 0.78, respectively. In particular, in October, the model aligns closely with observation as the salinity distribution features near-zero values within the lagoon. Low-frequency fluctuations in salinity, observed to shift between the low-water period (~25 psu) and the flood period (~0 psu), are accurately replicated by the model (Figure 5b). On a seasonal scale, the correlation coefficient, mean difference, standardized squared error, and ratio of standard deviations between the two timeseries are 0.97, 0.28 psu, 10%, and 0.98, respectively. These findings demonstrate the model's capability to faithfully reproduce the observed variations in salinity, both spatially and seasonally. Readers seeking more detailed information on the *Ref* simulation's capability to accurately model the spatio-temporal variability of the salinity at monthly scales are referred to Okpeitcha et al. (2024).

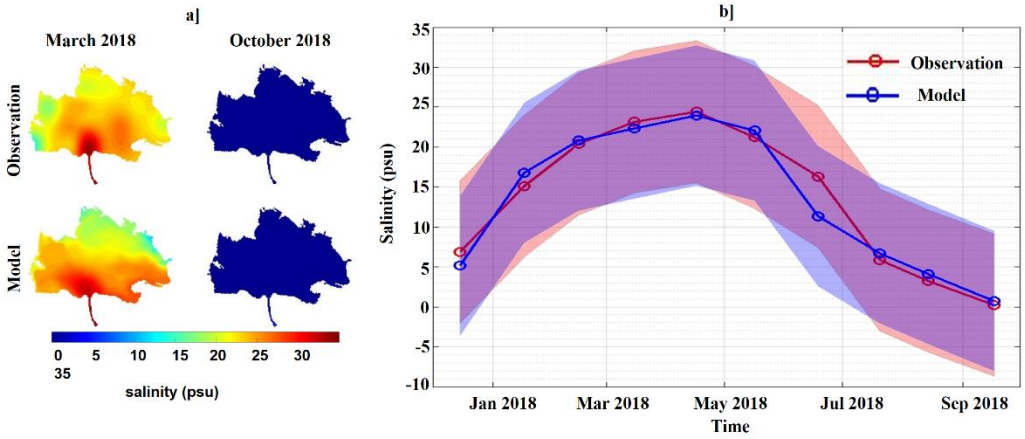

Figure 5: The salinity regime in the lagoon: a] Spatial distribution of observed (top row) and modeled (bottom row) surface salinity in March and October 2018; b] Monthly trend in mean salinity in the lagoon, for observations (red line) and model (blue line). Shaded areas correspond to ±1 standard deviation around mean values.

As evidenced above, the *Ref* simulation reproduces the major evolution patterns of observed flows, water levels, temperature, and salinity distribution within the lagoon (see also Okpeitcha et al., 2024). In particular, the satisfactory representation of spatio-temporal variability of salinity is of major importance when evaluating residence time using Eulerian or Lagrangian tracers. While acknowledging limitation in the model's representation of high-frequency currents in the Cotonou channel, whose possible impact is discussed in Section 4, the *Ref* simulation is estimated to give a satisfactory representation of the lagoon circulation and to be reliable for estimating residence time.

3.2. Lagoon circulation and sensitivity to different drivers

a- Seasonal circulation

Fig. 6 shows seasonal variations in surface (top panel) and bottom (bottom panel) circulations for four distinct periods. During the flood period (September-November), the substantial inflow of freshwater (~1200 m^3/s) from the Sô and Ouémé rivers results in relatively strong mean currents (>7 cm/s) within the lagoon, establishing a connection between the rivers and the Cotonou channel (Fig. 6a). The circulation pattern exhibits quasi-barotropic behavior, with bottom currents mirroring those at the surface, albeit at slightly reduced intensities (~4 cm/s) (Fig. 6e). Notably, the mean outflow through the channel is particularly vigorous during this phase of high water levels, with average surface outflow currents of approximately ~70 cm/s and bottom outflow currents of about ~35 cm/s. This pronounced outflow significantly curtails the impact of tidal influence in the southern part of the lagoon during this period.

Subsequent to the flood period, a transitional phase (December-January) occurs, characterized by a sharp reduction in freshwater inflow (~100 m^3/s, Fig. 2) and an increase in salinity (Fig. 5; Okpeitcha et al., 2022; 2024). During this period, surface circulation within the lagoon weakens significantly (~2 cm/s), though the connection between the rivers and the Cotonou channel remains discernible (Fig. 6b). Distinct recirculation cells become apparent to the southeast of the lagoon, implying water retention in that region. The circulation pattern exhibits vertical shear, with a surface outflow of approximately ~5 cm/s and a bottom inflow of around ~2 cm/s (Fig. 6f). This pattern is typical for stratified estuarine and lagoon circulations, where saltwater infiltrates in the bottom layer while freshwater flows seaward at the surface.

Throughout the low-water season (February-June), river discharge is minimal (<10 m^3/s, as indicated in Fig. 2), resulting in peak salinity levels (Fig. 5b; Okpeitcha et al., 2022; 2024). During this period, surface circulation becomes more complex, marked by the presence of numerous recirculation and water retention cells. These average recirculation cells typically exhibit scales on the order of few kilometers. Additionally, a northward current emerges along the western periphery of the lagoon (~3 cm/s), while discernible west-east connections establish in the central and southern sectors. Near the bottom, circulation maintains this complexity, albeit being influenced by an east-west current (~1 cm/s). Oceanic water inflow persists in the south-western region of the lagoon.

Finally, during the July-August desalination period (Fig. 6d), river inflow to the lagoon increase again (>100 m^3/s, Fig. 2), and the more direct connection between the rivers and the Cotonou channel are gradually re-established (~4 cm/s). At the bottom, circulation is similar to that observed during low-water periods, with an east-west flow (~1 cm/s) and a penetration of water from the Cotonou channel towards the south-west of the lagoon.

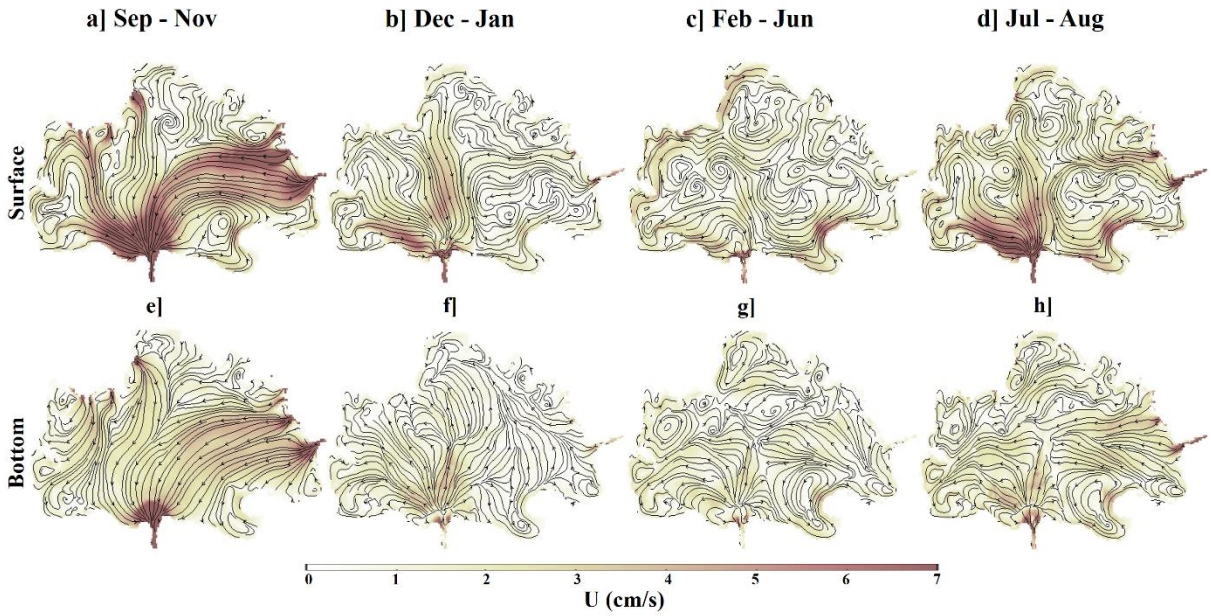

Figure 6: Mean seasonal surface (top panel) and bottom (bottom panel) circulation. a & e] flood period (September-November), b & f] salinization period (December-January), c & g] low-water period (February-June), d & h] desalination period (July-August). The colored background corresponds to current intensity, while streamlines are shown in black.

b- Sensitivity of lagoon circulation to wind, tide and salinity gradient

During the flooding period, prevailing winds across the lagoon primarily originate from the southwest as monsoon or trade winds, averaging around ~2.5 m/s. The *NoWind* simulation results in a ~1 cm/s increase in surface currents (Fig. 7b) and a ~1 cm/s decrease in bottom currents (Fig. 7f) compared to *Ref* (Fig. 7a and 7e). This significant difference is attributed to the wind-induced creation of a baroclinic circulation in the direction of the wind at the surface and in the opposing direction at the bottom (Bernardi et al., 2012; Cerralbo et al, 2016; Peng et al., 2021). This phenomenon moderates the north-south circulation on the surface and intensifies it at the bottom in *Ref*.

In contrast, the *NoTide* simulation (Fig. 7c and 7g) does not show a significant difference in circulation compared to *Ref* (Fig. 7a and 7e). However, the connection between the Sô and the Cotonou channel is slightly reinforced in the absence of tidal effects. This suggests that the tide tends to promote an average penetration of oceanic water predominantly from the southwest, as already noted above. In the case of the *NoSal* simulation (Fig. 7d and 7h), the exclusion of the salinity gradient influence within the forcings yields a minor decrease in surface circulation along the main current pathway connecting the Sô River to the Cotonou channel. Conversely, an increase in bottom currents is observed in the

438 southern part, in comparison to the *Ref* simulation (Figs. 7a and 7e). This underscores the role of the
439 salinity gradient in shaping the circulation, although its impact remains relatively minor.

440 During the flood period, freshwater inflow is the main driving force behind circulation, along with
441 wind, while the tide and salinity gradient play a lesser role in mean circulation.

442

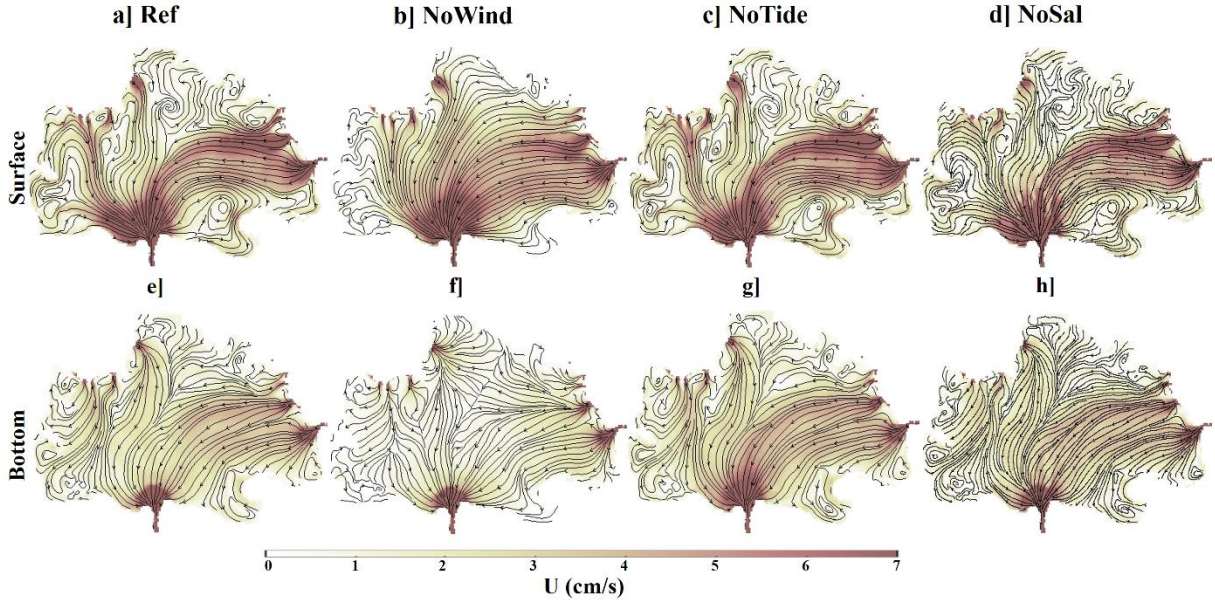

443

444 Figure 7: Influence of tide, wind and salinity gradient on surface and bottom circulation during flooding
445 (September-November): a & e] Simulation *Ref*, b &f] Simulation *NoWind*, c & g] Simulation *NoTide*, d
446 & h] Simulation *NoSal*. The majority of winds come from the south-west of the lagoon (averaging ~2.5
447 m/s). Average river discharge during this period is ~700 m^3/s.

448 During the salinization periods, river inflow significantly reduces (~100 m^3/s), and prevailing
449 winds maintain a southwestern direction at approximately 2.6 m/s (wind rose in Fig. 8). During this
450 phase, we observe only three occurrences of north-easterly wind events (harmattan), each lasting 1-3
451 days. Within this timeframe, the *NoWind* simulation (Fig. 8b) displays increased surface currents,
452 rendering the river-channel connections more pronounced than those in the *Ref* simulation (Fig. 8a). At
453 the bottom (Fig. 8f), changes in circulation are also apparent compared to the *Ref* scenario (Fig. 8e),
454 particularly in the northeastern area where bottom waters exhibit increased propagation towards the
455 channel in the *NoWind* case. Hence, winds once again dampen surface and bottom circulation, especially
456 in the northeastern region of the lagoon. In the *NoTide* simulation (Fig. 8c), surface recirculation and
457 water retention cells intensify in contrast to the *Ref* case (Fig. 8a), while at the bottom (Fig. 8g), the
458 absence of tidal effects leads to circulation patterns characterized by the emergence of east-west
459 connections. Similarly, the *NoSal* simulation (Figs. 8d and 8h) reveals that removing the salinity gradient
460 effect affects the circulation structure at both the surface and, more prominently, at the bottom, in

comparison to the *Ref* case (Figs. 8a and 8e). This shows that baroclinic flows induced by (horizontal and vertical) salinity gradients play a significant role, particularly at the bottom, in the progression of brackish water towards the eastern reaches of the lagoon.

Beyond the contribution of river inflows, the interplay of the tide, salinity gradient, and wind significantly shapes the circulation patterns during the salinization period. This results in surface and bottom exchanges between the lagoon and the ocean, as well as in the organization of circulation structures within the lagoon, including the emergence of east-west connections and the formation of recirculation cells.

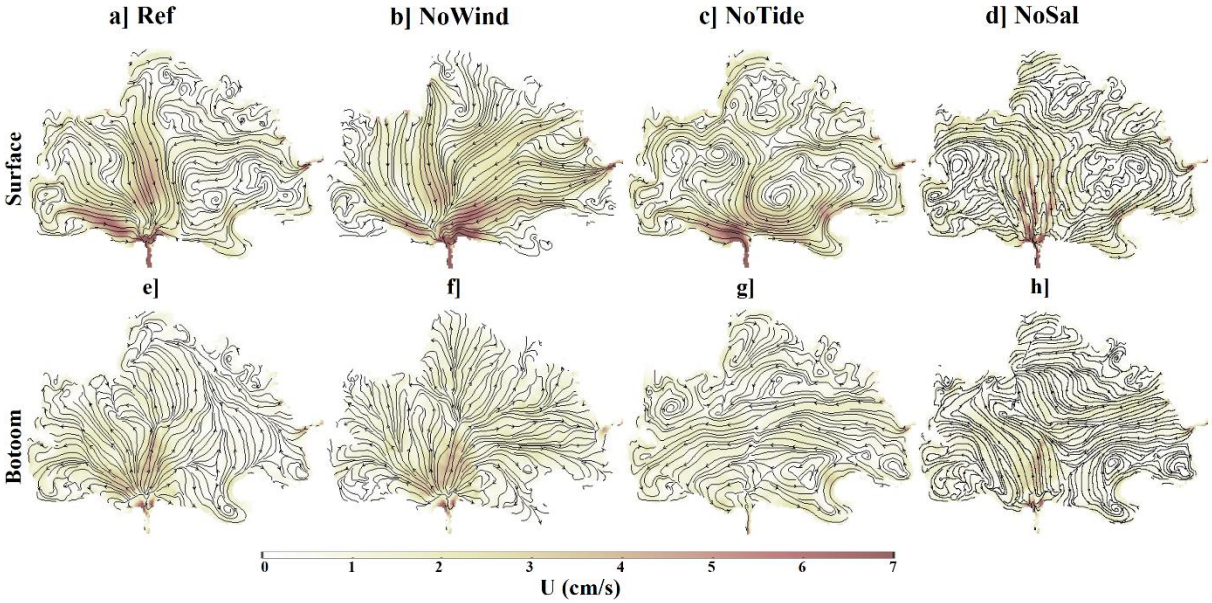

Figure 8: Influence of tide, wind and salinity gradient on surface and bottom circulation during salinization (December-January): a & e] Simulation *Ref*, b & f] Simulation *NoWind*, c & g] Simulation *NoTide*, d & h] Simulation *NoSal*. The majority of winds come from the south-west of the lagoon (averaging ~2.6 m/s). Average river inflow during this period is ~100 m^3/s.

During the low-water period (February-June), characterized by the lowest flows of the year (~10 m^3/s), prevailing winds average around ~3.3 m/s, predominantly from the southwest. The *NoWind* simulation (Fig. 9b) reveals a shift in the surface circulation pattern, marked by the emergence of river-channel connections and the vanishing of recirculation and water retention cells, contrasting with the *Ref* simulation (Fig. 9a). This implies that wind-induced circulation fosters instabilities and eddies, thereby promoting the emergence of recirculation zones at the surface (Fig. 9b). At the bottom (Fig. 9f), the *NoWind* simulation also leads to circulation alterations, including the dissolution of recirculation and retention cells. When eliminating the tide (*NoTide*), the surface circulation (Fig. 9c) remains largely unchanged compared to *Ref* (Fig. 9a), except in the vicinity of the channel where exchanges with the

ocean are considerably weaker. Meanwhile, the *NoTide* simulation (Fig. 9g) shows that the absence of tides marginally modifies the bottom circulation, reinforcing the observed east-west flow during this period (Fig. 9e). As for the *NoSal* simulation (Figs. 9d and 9h), the removal of salinity-dependent effects slightly enhances the complexity of the surface circulation structure, while at the bottom, the east-west flow gains some strength compared to *Ref* (Figs. 9a, 9e) during this interval. It is noteworthy that during this phase, the lagoon's salinity becomes more spatially uniform, with horizontal salinity gradients being less pronounced compared to the salinization period (Okpeitcha et al., 2022; 2024). Additionally, the efficacy of the wind-driven mixing process weakens the salinity gradient resulting from the convergence of modest river input and the saltier ocean water.

Consequently, wind influence emerges as the primary driver for lagoon circulation during the low-water period, particularly in terms of turbulence generation and the formation of recirculation structures. The effects of the tide and salinity gradient are small during this time of the year, except in the immediate vicinity of the channel.

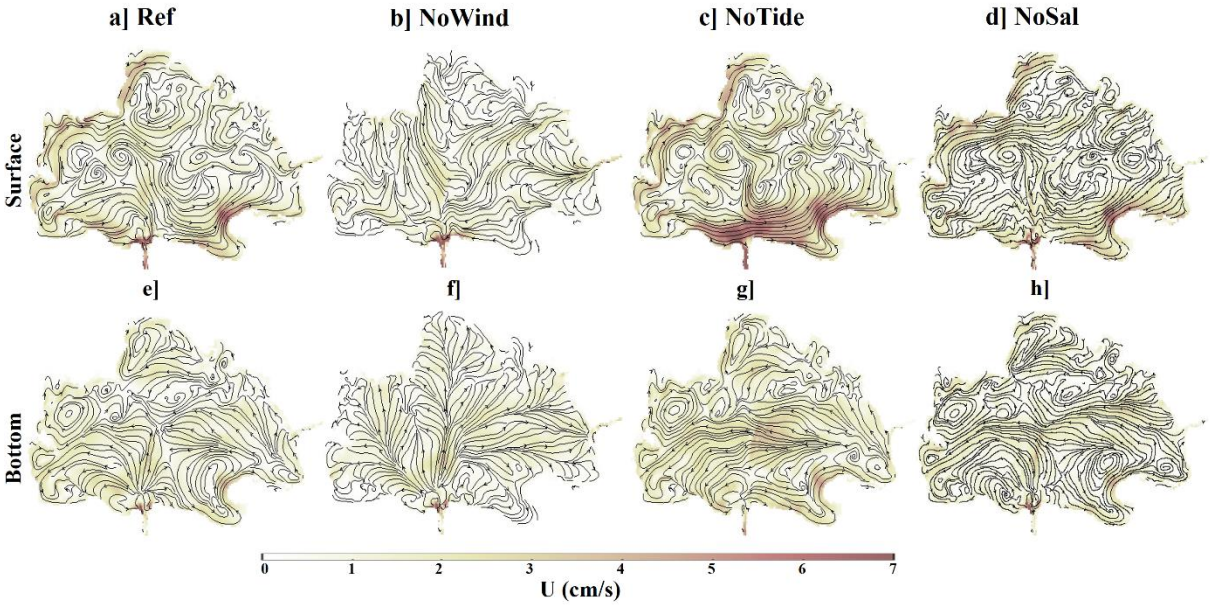

Figure 9: Influence of tide, wind and salinity gradient on surface and bottom circulation during low water (February-June): a & e] Simulation *Ref*, b & f] Simulation *NoWind*, c & g] Simulation *NoTide*, d & h] Simulation *NoSal*. The majority of winds come from the south-west of the lagoon (averaging ~3.3 m/s). Average river inflow during this period is ~10 m^3/s.

In the desalination period (July-August), river flow gradually increases (~200 m^3/s), accompanied by prevailing southwesterly winds with an average intensity of ~3.7 m/s (wind rose in Fig. 10). This period is marked by significant changes in circulation dynamics. The *NoWind* simulation (Fig. 10b) depicts a notable difference in current patterns, displaying a pronounced Ouémé-channel

connection compared to *Ref* (Fig. 10a). At the bottom (Fig. 10f), a dominance of water entry via the channel is observed, and the east-west flow component distinctive to *Ref* (Fig. 10e) vanishes. During this phase, winds notably attenuate surface circulation and reshape bottom currents, generating recirculation cells. The *NoTide* and *NoSal* simulations have relatively smaller effects on circulation. In the *NoTide* simulation (Fig. 10c), surface recirculation cells to the west of the lagoon gain slight intensity, inhibiting a more direct connection between the Sô and the channel seen in *Ref* (Fig. 10a). Meanwhile, at the bottom (Fig. 10g), the absence of tides leads to an enhanced river-channel connection compared to *Ref* (Fig. 10e). Similar to the tide, the *NoSal* simulation showcases a comparable influence due to the absence of the salinity gradient effect (Fig 10h).

In summary, during the desalination period, the interplay of wind and river inflow significantly shapes circulation patterns, with wind playing a decisive role. On the other hand, the tide and salinity gradient assume secondary roles in the circulation dynamics, similar to the low water period.

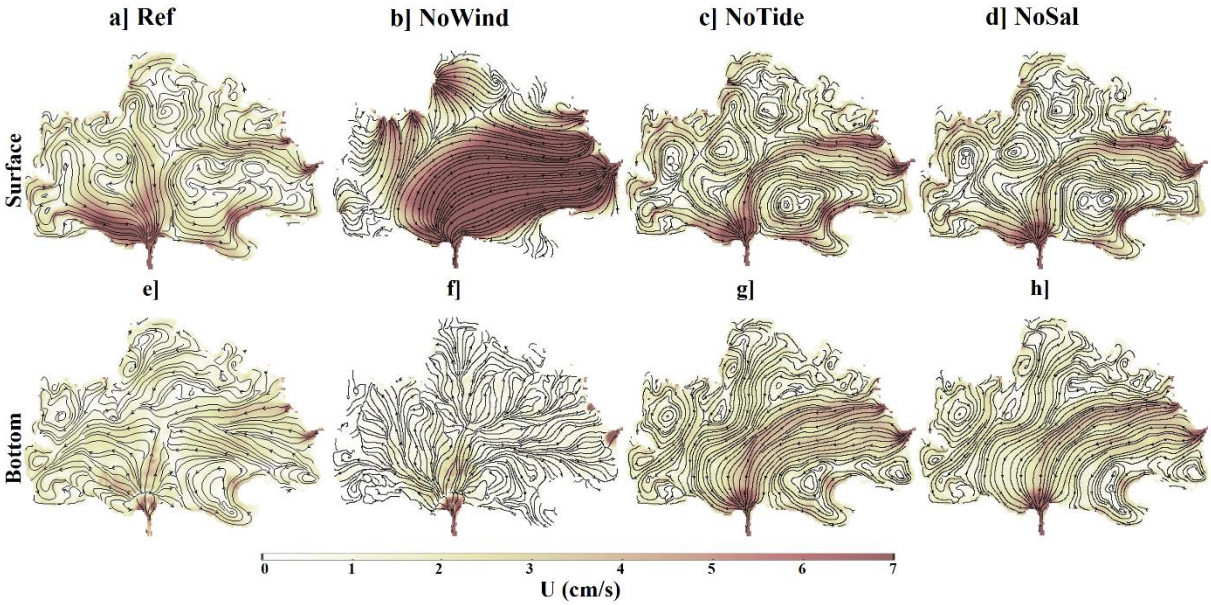

Figure (10): Figure 10: Influence of tide, wind and salinity gradient on surface and bottom circulation during desalination (July-August): a & e] Simulation *Ref*, b & f] Simulation *NoWind*, c & g] Simulation *NoTide*, d & h] Simulation *NoSal*. The majority of winds come from the south-west of the lagoon (averaging ~3.7 m/s). Average river inflow during this period is ~200 m^3/s.

3.3. Residence times of water masses in Nokoué Lagoon

a- Local residence time

Fig. 11 illustrates the spatial distribution of water mass residence times (T_R) for both surface and bottom layers, along with the corresponding mean circulation patterns, during various periods in the *Ref* simulation. During the flood season in October (Figs. 11a and 11e), surface and bottom water residence times are notably short (<7 days) across most of the lagoon. These short residence times result directly from the strong river inflow, establishing a direct link with the channel exit, as indicated by the previous circulation diagrams (Fig. 6a and 6e). However, sheltered areas in the north and south of the lagoon exhibit extended residence times (sometimes exceeding 1 month). As the salinization period commences in early December (Fig. 11b and 11f), the influence of river inputs partially diminishes, and the emergence of recirculation cells contributes to slightly longer residence times at both the surface (average ~18 days) and bottom (average ~17 days). Areas of water retention identified during the flood period expand, and new retention zones emerge at the lagoon's western and eastern edges. Moving into the low-water period in February (Fig. 11c and 11g), residence times for surface and bottom water reach several months (average ~123 days). Recirculation and retention cells span the entire lagoon, even extending far from the edges. With the exception of small regions close to the Cotonou channel or river mouths, residence times are uniform throughout the lagoon. Finally, as the desalination period initiates in early July (Fig. 11d and 11h), both surface and bottom water residence times significantly reduce again (average ~21 days for surface and ~20 days for bottom). This decrease is attributed to the increasing influx of river water, favoring reconnections to the ocean. As would be expected, longer T_R values correspond to periods characterized by recirculation cells, while shorter T_R values coincide with times of direct river-channel connections influenced by river inflows. Finally, it is also noteworthy that the average T_R across the lagoon remains nearly identical between the surface and the bottom, with only minor vertical disparities.

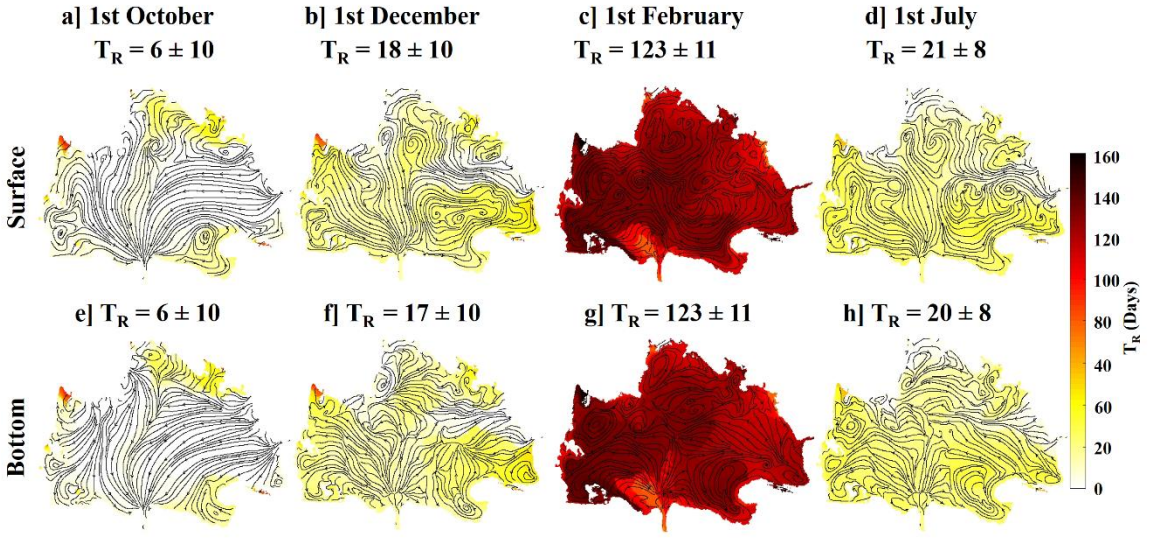

Figure 11: Local water-mass residence times (T_R, in days) and associated mean circulation. T_R were obtained for a passive tracer deployment on: a & e] 1st October, b & f] 1st December, c & g] 1st February, d & h] 1st July.

b- Seasonal cycle of mean residence times and sensitivity to different forcings

Fig. 12a shows the seasonal cycle of average residence times obtained in the *Ref* simulation at two-week intervals. This figure shows that during salinization and low-water periods (December-June), average T_R are much longer (4 to 1 month), due to low river inflows and complex circulation characterized by water retention cells. Conversely, during desalination and flood periods (July-November), average T_R contract to just a few days, attributable to strong freshwater influx from rivers and a nearly barotropic circulation oriented towards the ocean. Notably, the mean T_R exhibits a rapid and consistent decline from February to July.

Fig. 12b illustrates the impact of the main drivers (river inflow, tide, wind, and salinity gradient) on the mean T_R dynamics. From May to November, all simulations consistently yield similar average T_R values, associated with the sudden raise of the river flows and rapid flushing of the lagoon at the beginning of the wet season. In contrast from November to May, during the salinization and low water periods, T_R is more affected by other forcings. The *NoWind* simulation results in shorter residence times, reaching up to 50 days less than those of *Ref*. In contrast, the omission of the salinity gradient effect in the lagoon dynamics yields a mean T_R (*NoSal*) that surpasses mean T_R (*Ref*) by approximately 10 to 50 days. Similarly, when the tide is absent, the mean T_R (*NoTide*) extends by approximately 15 to 30 days compared to mean T_R (*Ref*) but only between December to February. Thus, winds and baroclinic effects related to salinity gradients have a more significant impact on the average T_R than the tide-induced circulation.

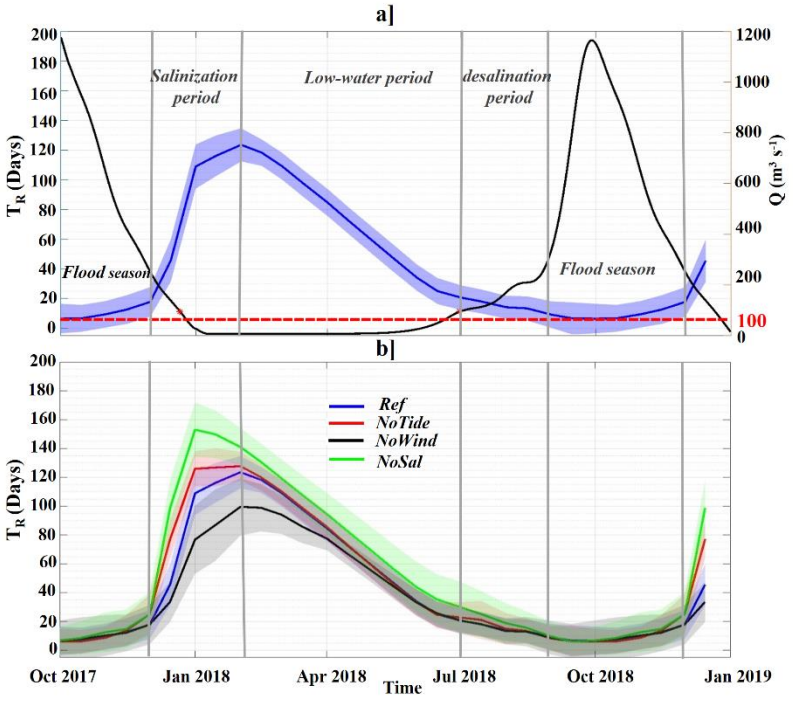

Figure 12: a] Seasonal cycle of the lagoon's mean surface residence time (in blue, the curve is very close for the bottom). River flows are shown in black (right axis), b] Sensitivity of mean surface residence time (T_R) in the lagoon to different forcings: *Ref (blue)*, *NoWind (black)*, *NoTide (red)* and *NoSal (green)*. Shaded areas correspond to ±1 standard deviation around the mean values.

4. Discussion

4.1. Seasonal circulation and residence times

The circulation patterns within the Nokoué Lagoon exhibit significant seasonal variations, primarily influenced by fluctuations in river flow. These seasonal shifts in circulation are also associated with marked variations in other parameters, such as water levels (Chaigneau et al., 2022; Morel et al., 2022), salinity (Okpeitcha et al., 2002; 2024), or turbidity of the water column (Ntangyong et al., under review). These fluctuations, directly influenced by seasonal monsoonal precipitation that drives river flow, strongly impact ecosystem characteristics and variability, from plankton (e.g. Chaigneau et al., 2023) to fish populations (Lalèyè et al., 1995; 2003; 2007). However, our results indicate that circulation patterns are further influenced, to varying degrees depending on the season, by additional factors such as oceanic tides, wind patterns, and baroclinic effects arising from salinity gradients. The seasonal circulation forced by these external factors significantly impacts the residence times of water-masses and tracers within the lagoon, as also suggested from salinity studies (e.g., Okpeitcha et al., 2024). This may have important implications for both pollutant dynamics and ecosystem equilibrium within the lagoon, associated with nutrient cycling and primary productivity (Lane et al., 2011; Rodhe, 1992).

For instance, our results highlight that during periods of low water, mean currents tend to be relatively weak. This weak circulation fosters the formation of recirculation cells that effectively trap water within the lagoon, thereby extending residence times to several months. These rather long residence times, could lead to pollutant accumulation, potentially posing risks to ecosystem health and biodiversity. Conversely, during high water periods, intensified and nearly barotropic currents are observed, establishing direct connections between the rivers and the Cotonou channel and facilitating the efficient discharge of water towards the ocean. This results in significantly shorter residence times, often spanning only a few days that may result in rapid flushing of pollutants, potentially reducing their accumulation and mitigating adverse effects on aquatic life.

Furthermore, the transition between these two seasonal extremes is characterized by a sharp and consistent decline in mean T_R from February to July. This linear trend underscores the role of river flow, particularly during the June-July period when discharge rates typically range from 50 to 100 m^3/s, in efficiently flushing water out of the lagoon and exerting dominant control over residence times even throughout much of the low-water season. Similarly, at the end of flood period, T_R begins to sharply increase when river discharge falls below approximately 100 m^3/s. These findings corroborate recent studies highlighting the existence of a critical threshold of river discharge, typically between 50-100 m3/s, necessary for effective lagoon flushing. For instance, using a simplified box model, Okpeitcha et al. (2022) estimated that a modest increase in river discharge of 10-15 m^3/s during the dry season could yield a substantial 30% reduction in salinity, with complete desalination occurring at discharge rates surpassing ~50-60 m3/s. Based on these results, Okpeitcha et al. (2024) used the realistic SYMPHONIE model and similar simulations than used here, revealing that river discharge exceeding 100 m3/s rapidly reduced average salinity to below ~5 within few days, aligning closely with the abbreviated residence times observed in the present study.

4.2. Impact of external drivers and identified limitations

Our results emphasized the impact of external forcings, (tides, winds, and salinity gradients) on average T_R, particularly during the salinization and low water periods spanning from November to May. Winds play a role in retaining water masses within the lagoon, while river inflow, tides, and salinity gradients promote evacuation. We will now briefly discuss each mechanism separately and highlight some limitations of our simulations.

The *NoTide* simulation results in longer T_R, extending from 15 to 30 days beyond those of the *Ref* simulation during December-January, with the most significant disparities observed at the onset of the salinization phase in December (Figure 12). This underscores the significant role of tide-induced flow in facilitating partial water renewal within the lagoon, particularly near the mouth of the Cotonou channel, where tidal influence is most pronounced. Non-linear interactions among tides, river flow, and

friction within the Cotonou channel influence fluxes (e.g., Morel et al., 2022) and thus T_R. Notably this mostly leads to a delay in T_R increments when tides are considered (Figure 12). This 2-month period (December-January) corresponds to the adjustment time of the lagoon under the tidal effect, before the average salinity of the lagoon reaches equilibrium (Okpeitcha et al., 2024).

As explained above, the present simulations considered an a typical roughness parameter Z_0 for which tidal flows in the Ref simulation appear stronger than those observed from ADCP data (Fig. 2), so that the Ref simulation overestimates the effect of tides. As discussed above, this effect is limited to the beginning of the salinization period and increases exchanges mostly near the channel mouth. A more realistic global T_R evolution curve would thus lay somewhere between the blue and red curves on Fig. 12. We limited the scope of the study to the present simulations, but to further limit the tidal fluxes in the channel, additional work is necessary and several approaches are possible. First, increasing Z_0 within the channel is the first obvious choice, but the present value leads to equivalent bottom friction that are already pretty high in the channel ($C_D \sim 5.\ 10^{-3}$). Higher values can thus become unrealistic and has also limited impact on the fluxes since, in our baroclinic simulations, velocity reduction by bottom roughness is limited to the bottom boundary layer, whose thickness is determined by the turbulent closure scheme. Thus using alternative closure schemes, more adapted to represent the effect and extension of the turbulent bottom boundary layer, is probably necessary too. Another possibility is to modify the water depth. The channel being narrow, the strong lateral depth variations are not well represented in the model. Increasing the resolution requires much more computation time, but it is possible to modify the bathymetry (slightly decrease the depth in some areas) to limit the fluxes. Finally, it may also be important to consider the dissipation and limitation of fluxes associated with bridge pillars (there are three bridges along the channel). In a structured grid model such as SYMPHONIE this can be done by imposing frictional effects over the whole water column close to each pillar position, but the tuning of the frictional coefficient is unclear for now.

In a similar context, it is important to highlight the presence of artificial fishing parks, referred to as "acadjas" (Chaffra et al., 2020; Niyonkuru et Lalèyè, 2010; Welcomme, 1972), within the lagoon. These acadjas are composed of a multitude of branches and aim to mimic the natural mangrove habitat. Occupying approximately 16% of the total area of the lagoon (Chaffra et al., 2020), these artificial structures provide refuge and breeding areas for fishes (Villanueva et al., 2006). However, it is important to consider the physical implications of these structures, as they are likely to impede surface winds and induce additional dissipation in the water column. While our study did not incorporate this dissipation due to the intricate nature and small size of the individual brush parks, it could potentially impact the lagoon's hydrodynamics. Therefore, further model calibration studies would be necessary to fine-tune the simulations and achieve even more accurate results by accounting for dissipation in both the Cotonou channel and that induced by the acadjas within the lagoon.

669 During periods of salinization and low water levels, the *NoSal* simulation exhibited longer T_R,
670 extending by approximately 10 to 50 days compared to those of the *Ref* simulation. This underscores
671 the significant contribution of baroclinic flows driven by salinity gradients to the replenishment of water
672 masses within the lagoon. Okpeitcha et al. (2024) observed that this baroclinic circulation increases salt
673 influx at the mouth of the channel in the southern part of the lagoon, and facilitates its redistribution
674 throughout the lagoon via high-frequency processes. Consequently, without the influence of salt
675 gradients, the lagoon experiences a lower increase in salinity (Okpeitcha et al., 2024), indicative of its
676 tendency to retain fresh waters and thereby prolong the residence time.

677 In contrast, the *NoWind* simulation demonstrates shorter T_R, ranging from 2 to 50 days less than
678 those of the *Ref* simulation, indicating that wind plays a role in enhancing water retention within the
679 lagoon. With the prevailing southwest wind regime, wind-induced circulation tends to counteract the
680 flow induced by river discharge, typically oriented from north to south in the lagoon. These wind-
681 induced currents generate a baroclinic circulation pattern characterized by a surface current aligned with
682 the wind direction and a reverse flow at the bottom. This finding is consistent with similar observations
683 reported in other studies (e.g., Bernardi et al., 2012; Cerralbo et al., 2016; Lacy et al., 2003; O'Callaghan
684 and Stevens, 2011). Furthermore, the wind-induced circulation, in conjunction with its non-linear
685 interaction with tides and baroclinic gravity currents, fosters mesoscale instabilities that contribute to
686 water retention. Interestingly, as previously highlighted by Okpeitcha et al. (2024) based on salinity
687 analysis, an additional simulation (not presented here) driven by seasonal (low-frequency) winds yielded
688 a circulation and T_R very similar to the *Ref* simulation. This suggests that the high-frequency variations
689 of wind play a minor role in the lagoon's circulation dynamics. This unexpected finding suggests that
690 the persistent winds generate small-scale circulations, potentially through shear instabilities or under the
691 influence of topography. This is confirmed by Figs. 7-10 which exhibit the generation of mean
692 horizontal recirculation patterns at a small scale when considering the influence of wind, whereas these
693 features are absent in the *NoWind* configuration. This eddying circulation, induced primarily by low-
694 frequency southwest winds, contributes to increased retention and T_R within the lagoon, as well as to
695 the redistribution of salt (Okpeitcha et al., 2024).

696 In this study, we utilized wind forcing with a relatively coarse spatial resolution of ¼° (~25 km)
697 from ECMWF, which was then interpolated onto our simulated domain. However, numerous studies
698 have highlighted the significant impact of wind spatial resolution on surface dynamics in semi-enclosed
699 basins or coastal oceans (Duy et al., 2022; Cerralbo et al, 2016). Given that wind plays a crucial role in
700 influencing the circulation and residence times (T_R) of the Nokoué Lagoon, future investigations should
701 explore the sensitivity of lagoon dynamics to the spatial resolution of wind data. Additionally, our
702 simulations did not incorporate wave dynamics and its influence on the circulation. Although wave
703 characteristics in the Nokoué Lagoon remain undocumented, recent field observations suggest typical

significant wave heights of 0.2 m, with an increase to 0.4 m during the afternoon, possibly influencing the circulation and residence times.

4.3. *Relationship between mean residence times and lagoon flushing times*

As previously mentioned, various time scales can be used to estimate water retention in coastal systems (e.g., Zimmerman, 1976; Takeoka, 1984; Monsen et al., 2002). Here, we compare and discuss the results obtained from local residence times (T_R), derived from the decrease of tracer concentration in the Nokoué Lagoon, with flushing times (T_f), which characterize the overall exchange properties of the lagoon.

Flushing time (T_f) is a commonly used metric for assessing water renewal in a lagoon, representing the duration required to completely replace the volume of water in the system. This renewal process involves incoming flows (*Qe*) from rivers and outgoing flows (*Qs*) through the channel connecting the lagoon to the ocean (e.g., Andréfouët et al., 2001; Geyer et al., 2000). Under steady-state conditions and assuming instantaneous and thorough mixing of water within the lagoon (essentially functioning as a continuously stirred tank), $Qe = Qs = Q$, and tracer concentration in the lagoon decrease exponentially at a rate given by the timescale $T_f = V/Q$, where V denotes the volume of water in the lagoon (Umgiesser et al., 2014; Du et al., 2016; Monsen et al., 2002; Koutitonsky et al., 2004; Dyer, 1973). Interestingly, this also corresponds to the time necessary to entirely empty the lagoon if water flows unidirectionally from the entrance to the outlet without mixing, effectively pushing the water within the lagoon towards the outlet like a piston.

Applied to the Nokoué Lagoon, T_f would be approximately 340 days during the low water period (with $V \sim 2.35 \times 10^8$ m^3 and $Q \sim 8$ m^3/s), and less than 4 days during the flood season (with $V = 3.25 \times 10^8$ m^3 and $Q \sim 1100$ m^3/s). These calculated T_f values are significantly longer than the T_R values obtained during low water periods. This disparity arises from the strong and erroneous assumptions of stationarity and homogeneity. Indeed, first in the Nokoué Lagoon the circulation patterns is complex (exhibiting retention areas and strong spatial variations of mixing properties within the lagoon) but second and of primary importance river discharge, water levels, and consequently volume significantly vary over time on much shorter scales than the estimated T_f (e.g., Chaigneau et al., 2022; Morel et al., 2022).

Therefore, it is imperative to take into account the non-stationarity of the system and the notable volume and discharge fluctuations during the emptying phase. In this case, the change in volume is mathematically represented as follows:

$$\frac{dV}{dt} = \mathrm{Q}_e - \mathrm{Q}_s \qquad (1)$$

By definition of the flushing time in the no mixing context, we have:

738 $$\int_t^{t+T_f} \mathrm{Q}_s \, \mathrm{dt} = \mathrm{V(t)} \qquad (2)$$

739 Using equation (1):

740 $$\int_t^{t+T_f} (\mathrm{Q}_e - \frac{dV}{dt}) \, \mathrm{dt} = V(t) \qquad (3)$$

741 This gives :

742 $$\int_t^{t+T_f} \mathrm{Q}_e \, \mathrm{dt} = \mathrm{V(t + T}_f) \qquad (4)$$

743 This final equation signifies that the flushing time aligns with the moment when the quantity of water
744 introduced into the lagoon by the rivers within the time interval from t to $t+T_f$ becomes equivalent to
745 the lagoon's volume V. Knowing $Q_e(t)$ and $V(t)$, both of which can be assessed at each model time step,
746 equation (4) allows to compute the flushing time along with its temporal evolution. A similar approach
747 can be used in the context of complete mixing and it can be shown that similarly to the traditional
748 definition the refined calculation of T_f proposed here corresponds to both the timescale of an exponential
749 decrease in the context of complete mixing in the lagoon or to the timescale of entire emptying in the
750 context of no mixing, taking time evolution of the fluxes into account.

751 Fig. 13 shows the seasonal cycle of both the obtained flushing time (T_f) and the average
752 residence times T_R, estimated at two key points: when the initial tracer concentration decreases to an
753 exponential factor (1/e ~ 36.8%, as depicted in Fig. 12a), and when it diminishes to 5% of its initial
754 value, a situation for which the lagoon is almost entirely emptied from its initial waters. At the lagoon
755 scale, the flushing time T_f (red curve) varies from a few days to 6 months in connection with the
756 hydrological cycle. The lagoon thus rapidly renews during flood periods (~3 days), while during periods
757 of salinization and low-water, this time is much longer (up to 6 months) due to low river flows. A steady
758 decrease slope of T_f (from ~5 to ~1 month) is noticeable between February and July, indicating once
759 again the predominant role of June-July river flows in lagoon flushing during the low-water season.
760 Indeed, the waters tend to remain trapped in the lagoon (very long T_f and T_R) until the threshold flow is
761 reached (in July) at ~50-100 m^3/s (Figure 12a), beyond which the lagoon's water is rapidly renewed.
762 This is consistent with the critical flow rate of ~ 60 m^3/s estimated by Okpeitcha et al. (2022) from
763 observations of salinity variations.

764 Both T_f and T_R (1/e) exhibit similar seasonal variations, yet T_f, here associated with the
765 exponential decay and complete mixing context, significantly exceeds T_R (1/e) during periods of low
766 water. T_R (1/e) < T_f can be expected since river waters only gradually mix with waters from the rest of
767 the lagoon, so that there is a delay for mixed waters to reach the channel mouth, depending on the
768 circulation intensity at the lagoon scale. The difference reaching up to 3 months during the salinization

period, this indicates very weak circulation and exchanges within the lagoon in the low water season. Alternatively, Fig. 13 also shows that T_f, now associated with the entire flushing in the no mixing context, is always below T_R 5% (the time required to achieve a 95% -almost complete- decrease of the initial tracer concentration). This is again expected since the occurrence of mixing in the lagoon induces retention of initial waters in the lagoon. Notably, aside from the sharp increase period observed in December, the difference between T_f and T_R 5% remains relatively constant, typically spanning 20-30 days, indicating that mixing tends to prolong the retention of tracers by approximately 1 month.

To conclude, the circulation is the major ingredient controlling the residence time in the lagoon: it is intense in the wet season, connecting river mouths to the channel and the ocean, leading to a rapid flushing of the lagoon. It is weak during the low water season, leading to residence times controlled by the arrival of the first river floods at the beginning of the wet season. Mixing at local scales has a significant impact on the residence time at the beginning of dry season, extending it by about 1 month. Flushing time calculation proposed here, which incorporate variable flows and volumes, offer more precise estimates compared to those relying on assumptions of stationarity. Additionally, other significant metrics and methodologies for pollutant monitoring can be employed, such as those using Lagrangian transport. In these approaches, local residence times are defined at specific points in the lagoon as the transit time of particles from each location to the channel outlet (Delhez et al., 2014; Cucco et al, 2009). These diagnostics can provide additional insights beyond the Eulerian diagnostics used here and warrant further exploration in future research to achieve a comprehensive understanding of the residence time characteristic of the Nokoué Lagoon.

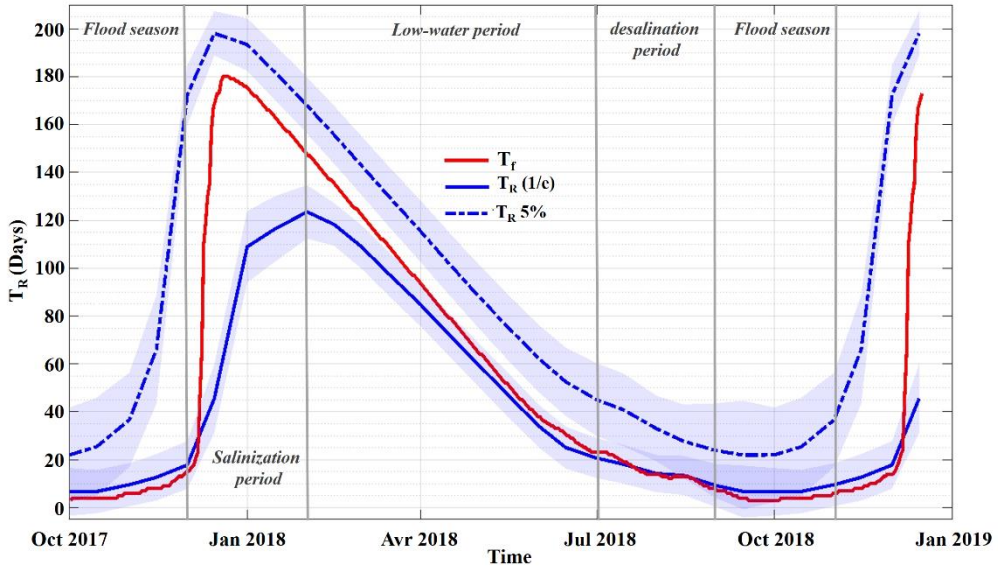

Figure (13): The seasonal cycle of flushing time T_f (red curve) and average residence time T_R corresponding to the time for the initial concentration to decreases to an exponential factor (1/e ~ 36.8%), and 5%.

5. Conclusion

This study used advanced numerical simulations from the SYMPHONIE model to achieve three key objectives: investigating seasonal circulation variations in the Nokoué Lagoon, identifying the driving factors of the circulation fluctuations, and quantifying residence times.

The high-water period (September-November) features direct river-channel connections driven by significant river inflow and wind dynamics, resulting in a 8-day average residence time. During the salinization phase (December-January), a two-layer estuarine circulation pattern develops, influenced by tide, salinity gradient, and wind. During this phase, water residence times within the lagoon increase to ~4 months. The low-water period (February-June) exhibits wind-driven recirculation cells and residence times of 1-4 months. The desalination period (July-August) brings back direct river-channel connections, reducing residence times to 20 days. Figure 14 provides a succinct summary of the average lagoon circulation and residence time on a seasonal scale. Key findings highlight a critical flow threshold of ~50-100 m^3/s in June-July, above which the lagoon experiences a rapid water renewal and controlling the residence time of waters for most of the preceding low water season. Sensitivity analyses emphasize the southwest wind's role in retaining water during the salinization and low-water periods (December-June), while river inflow, tide, and salinity gradient promote water evacuation during the desalination and high-water periods (July-December). We have also identified weaknesses in our simulations, which are not expected to drastically modify our conclusions, but it seems interesting to refine the dissipation of tides within the Cotonou channel or to better incorporate the influence of fishing parks on wind and currents due to fishing parks within the Lagoon.

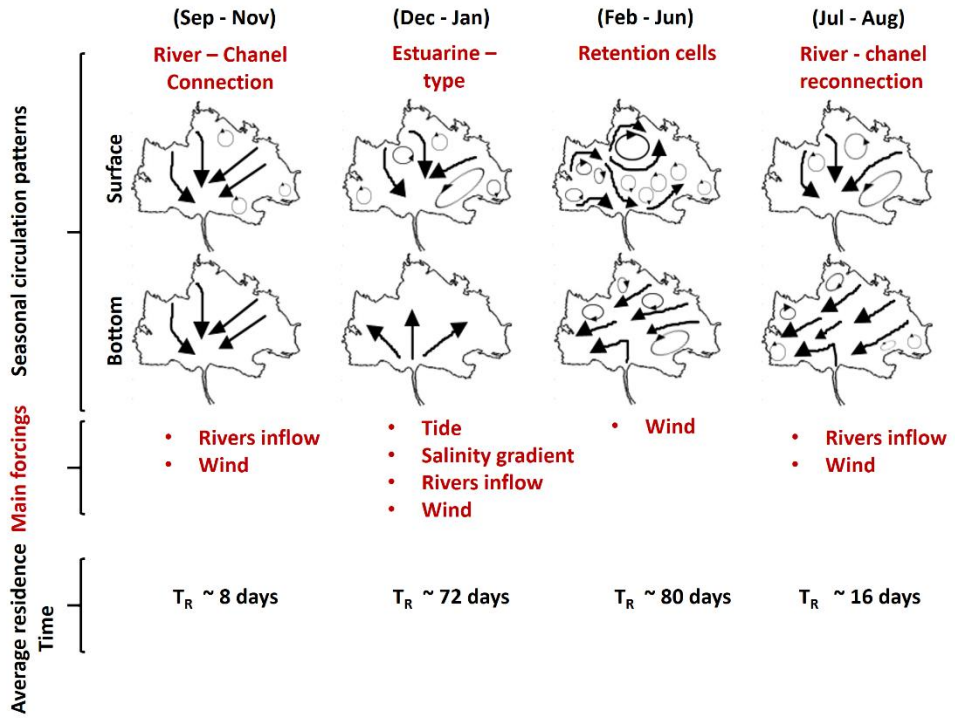

Figure 14: Graphical abstract of average seasonal traffic patterns and average seasonal residence time.

Our findings indicate potential risks of pollutant accumulation, particularly during low-water periods (December-June) when water residence times can extend for several months. This risk is most pronounced along the lagoon's shorelines, where contaminant inputs are more likely to occur. These results have significant implications for understanding the dynamics of the Nokoué Lagoon and, importantly, for predicting the fate of contaminants. While our Eulerian residence time approach offers valuable insights, augmenting it with a Lagrangian perspective - tracing water parcel trajectories until exiting the study area – could lead concrete understanding of particulate and dissolved waste residence times originating from lakeside villages and urbanized shores. In the future, like many other coastal zones, Nokoué Lagoon and its watershed are expected to experience a significant increase in human impact, including dredging, construction of artificial islands, installation of dams, and flow regulation measures. The simulations developed in our study offer a framework for evaluating the impact of such developments on lagoon ecosystem functioning, thereby facilitating decision-making processes.

Acknowledgements

The in situ data used in this study were collected by the Nokoué team, funded by IRD (Institut de Recherche pour le Développement) and IRHOB (Institut de Recherches Halieutiques et Océanologiques du Bénin). Numerical simulations were carried out using the facilities of the CALMIP HPC computing center (projects P18033, P1325, P13120) and the authors would like to thank the SIROCCO Code Community (CC) SIROCCO (https://sirocco.obs-mip.fr/). J. HONFO was funded through a scholarship

grant of the IRD. This work is a contribution to the « JEAI SAFUME » project funded by IRD and to the "Lagune Nokoué" TOSCA project funded by the French National Center for Space Studies (CNES). Finally, the comments of 2 anonymous reviewers helped improving the presentation and discussion section of the paper, in particular concerning the flushing time analysis and the dissipative processes within the Cotonou channel.

842 ***References***

Abdelrhman A. M. (2002). Modeling How a Hurricane Barrier in New Bedford Harbor, Massachusetts, affects the hydrodynamics and residence Times. Estuaries, 25 (2) , 177-196. https://link.springer.com/article/10.1007/BF02691306

Adite A., Winemiller K. O. (1997). Trophic ecology and ecomorphology of fish assemblages in coastal lakes of Benin, West Africa. ECOSCIENCE, 4(1), 6-23. https://doi.org/10.1080/11956860.1997.11682371

Adite A., Sonon S. P., Gbedjissi G. L. (2013). Feeding ecology of the mangrove oyster, Crassostrea gasar (Dautzenberg, 1891) in traditional farming at the coastal zone of Benin, West Africa. Natural Science, 5(12), 1238-1248. http://dx.doi.org/10.4236/ns.2013.512151

Adjahouinou D.C., Liady N. D., Fiogbe E. D. (2012). Diversité phytoplanctonique et niveau de pollution des eaux du collecteur de Dantokpa (Cotonou-Bénin). International Journal of Biological and Chemical Sciences, 6(5), 1938-1949. http://dx.doi.org/10.4314/ijbcs.v6i5.4

Adjahouinou D.C., Yehouenou B., Liady M. N. D., Fiogbe E. D. (2014). Caractérisation bactériologique des eaux résiduaires brutes de la ville de Cotonou (Bénin). Journal of Applied Biosciences, 78, 6705-6713. http://dx.doi.org/10.4314/jab.v78i1.13

Aina M.P., Djihouessi B., Vissin E.W., Kpondjo N.M., Gbèdo, V., Sohounhloué, K.C.D. (2012a). Characterization of the domestic wastewaters and dimensionality of a pilot treatment station by lagooning at Abomey Calavi city- Benin. International Journal of Engineering Science, 1(1), 45-50.

Aina M. P., Degila H., Chikou A., Adjahatode F., Matejka, G. (2012b). Risk of intoxication by heavy metals (Pb, Cd, Cu, Hg) connected to the consumption of some halieutic species in lake Nokoué: case of the Penaus schrimps and the Sarotherodon Melanoth. British Journal of Science, 5(1), 104-118.

Allersma E., Tilmans W.M.K. (1993). Coastal conditions in West Africa: a review. Ocean & Coastal Management, 19, 199-240. https://doi.org/10.1016/0964-5691(93)90043-X

Andréfouët S., Pagès J., Tartinville B. (2001). Water renewal time for classification of atoll lagoons in the Tuamotu Archipelago (French Polynesia). Journal International Coral Reefs, 9, 399-408. https://link.springer.com/article/10.1007/s00338-001-0190-9

Arakawa A., Lamb V.R. (1977). Computational Design of the Basic Dynamical Process of the UCLA General Circulation Model. Methods Computational Physics, 17, 173-265. http://dx.doi.org/10.1016/B978-0-12-460817-7.50009-4

Auclair F., Marsaleix P., Estournel C. (2001). Specification of the exchanges through the continental shelf break in high resolution coastal models: penetration of the LPC current over the Gulf of Lion (Mediterranean). Oceanol. Acta 24 (6), 529–544.

Avigdor A., Denny M. (1997). Settlement of Marine Organisms in Flow. Annual Review of Ecology and Systematics, 28(1), 317-339. https://doi.org/10.1146/annurev.ecolsys.28.1.317

Balotro R. S., Isobe1 A., Shimizu M. (2003). Seasonal Variability in Circulation Pattern and Residence Time of Suo-Nada. Journal of Oceanography, 259-277. http://dx.doi.org/10.1023/A:1025555608384

Baohong C., Weidong J., Jinmin C., Cai L., Haining H., Yunlong H., Xianbiao J. (2013). Characteristics of nutrients in the Jiulong River and its impact on Xiamen water, China. Chinese Journal of Oceanology and Limnology, 31, 1055-1063. http://dx.doi.org/10.1007/s00343-013-2263-3

Béjaoui B., Solidoro C., Harzallah A., Chevalier C., Chapelle A., Zaaboub N., Aleya L.. (2016). 3D modeling of phytoplankton seasonal variation and nutrient budget in a southern Mediterranean Lagoon. Marine Pollution Bulletin, 1-15. http://dx.doi.org/10.1016/j.marpolbul.2016.11.001

Blumberg A. & Mellor G. (1987). A description of a three-dimensional coastal ocean circulation model, three-dimensional coastal ocean models. Coastal Estuarine Sci. http://dx.doi.org/10.1029/CO004p0001

Bolin B. and Rodhe H.. (1973). A note on the concepts of age distribution and transit time in natural reservoirs. 25 (1), 58-62. https://doi.org/10.1111/j.2153-3490.1973.tb01594.x

Bouchette F., Schuster M., Ghienne J-F., Denamiel C., Roquin C., Abderamane M., P. Marsaleix, P. Duringer P. (2010). Hydrodynamics in Holocene Lake Mega-Chad. Quaternary Research, 73(2), Pp. 226-236. https://doi.org/10.1016/j.yqres.2009.10.010

Bretherton F. P., Russ E. D. And Fandry C. B.. (1976). A technique for objective analysis and design of oceanographic experiments applied to MODE-73. Deep-Sea Research, 23, 559-582. https://doi.org/10.1016/0011-7471(76)90001-2

Cerralbo P., Manuel Espino, Manel Grifoll. (2016). Modeling circulation patterns induced by spatial cross-shore wind variability in a small-size coastal embayment. Ocean Modelling, 104, 84-98. http://dx.doi.org/10.1016/j.ocemod.2016.05.011

Chaigneau A., Ouinsou T. F., Akodogbo H. H., Dobigny G., Avocegan T. T., Dossou-Sognon F. U., Okpeitcha V O., Djihouessi M. B. and Azémar F. (2023). Physicochemical Drivers of Zooplankton Seasonal Variability in a West African Lagoon (Nokoué Lagoon, Benin). Journal of Marine Science and Engineering, 11(556), 1-24. https://doi.org/10.3390/jmse11030556

Chaigneau A., Okpeitcha O. V., Morel Y., Stieglitz T, Assogba A., Benoist M., Allamel P., Honfo J., Sakpak D. A. T., Rétif F., Duhaut T., Peugeot C., Sohou Z. (2022). From seasonal flood pulse to seiche: Multi-frequency water-level fluctuations in a large shallow tropical lagoon (Nokoué Lagoon, Benin). Estuarine, Coastal and Shelf Science, 267 (107767),1-12. https://doi.org/10.1016/j.ecss.2022.107767

Chaffra A.S., A.C. Agbon, E.A.M. Tchibozo (2020). Cartographie par télédétection des Acadjas, une technique de pêche illicite sur le lac Nokoué au Bénin. Sci. Tech., 5, 11–29.

Costa A., Doglioli A. M., Marsaleix P., Petrenko A. A. (2017). Comparison of in situ microstructure measurements to different turbulence closure schemes in a 3-D numerical ocean circulation model. Ocean Modelling, 1-17. https://doi.org/10.1016/j.ocemod.2017.10.002

Cucco A., Umgiesser G. (2006). Modeling the Venice Lagoon residence time. Ecological Modelling, 193, 34-51. https://doi.org/10.1016/j.ecolmodel.2005.07.043

Cucco A., Umgiesser G., Ferrarin C., Perilli A., Canu D. M., Solidoro C. (2009). Eulerian and lagrangian transport time scales of a tidal active coastal basin. Ecological Modelling, 220, 913-922. https://doi.org/10.1016/j.ecolmodel.2009.01.008

Bernardi D., Caleffi V., Gasperini L., Schippa L., Valiani A. (2012). A Study of the Hydrodynamics of the Coastal Lagoon “Valli di Comacchio”. 3Rd Symp.int. on Shallow Flows, Iowa City, USA, 1-11.

Delhez E. M., Heemink, A.W., Deleersnijder, E. (2004). Residence time in a semi-enclosed domain from the solution of an adjoint problem. Estuarine, Coastal and Shelf Science , 61, 691-702. https://doi.org/10.1016/j.ecss.2004.07.013

Delhez E. M., de Brye B., de Brauwere A., Deleersnijder E.. (2014). Residence time vs influence time. Journal of Marine Systems, 132,185-195. http://dx.doi.org/10.1016/j.jmarsys.2013.12.005

Djihouessi M. B., Djihouessi M. B., Aina M P. (2019). A review of habitat and biodiversity research in Lake Nokoueé, Benin Republic : Current state of knowledge and prospects for further research. Ecohydrology & Hydrobiology, 19, 131–145. https://doi.org/10.1016/j.ecohyd.2018.04.003

Djihouessi M. B., Aina M. P. (2018). A review of hydrodynamics and water quality of Lake Nokoué : Current state of knowledge and prospects for further research. Regional Studies in Marine Science, 18, 57–67. https://doi.org/10.1016/j.rsma.2018.01.002

Djihouessi M. B., Aina M.P., Kpanou B., Kpondjo N. (2017). Measuring the Total Economic Value of Traditional Sand Dredging in the Coastal Lagoon Complex of Grand-Nokoué (Benin). Journal of Environmental Protection, 8, 1605-1621. https://doi.org/10.4236/jep.2017.813099

Dovonou F., Aina M., Boukari M. et Alassane A. (2011). Physico-chemical and bacteriological pollution of an aquatic ecosystem and its ecotoxicological risks: the case of Lake Nokoue in southern Benin. International Journal of Biological and Chemical Sciences, 5(4), 1590-1602. http://dx.doi.org/10.4314/ijbcs.v5i4.23

Dyer, K. R. 1973. Estuaries: A Physical Introduction, 1st edition. John Wiley and Sons, London, U.K.

Du J., Shen J. (2016). Water residence time in Chesapeake Bay for 1980–2012. Journal of Marine Systems 164, pp 101–11. http://dx.doi.org/10.1016/j.jmarsys.2016.08.011

Duy T. T., Herrmann M., Estournel C., Marsaleix P., Duhaut P., Hong L.B., Bich N. T. (2022). The role of wind, mesoscale dynamics, and coastal circulation in the interannual variability of the South Vietnam Upwelling, South China Sea – answers from a high-resolution ocean model. Ocean Sci., 18, 1131–1161. https://doi.org/10.5194/os-18-1131-2022

Estournel C., Bosc E., Bocquet M., Ulses C., Marsaleix P., Winiarek V., Osvath I., Nguyen C., Duhaut T., Lyard F., Michaud H., and Auclair F. (2012). Assessment of the amount of cesium-137 released into the Pacific Ocean after the Fukushima accident and analysis of its dispersion in Japanese coastal waters. Journal of Geophysical Research, 117, C11014. https://doi.org/10.1029/2012JC007933

Estournel C., Zervakis V., Marsaleix P., Papadopoulos A., Auclair F., Perivoliotis L., Tragou E (2005). Dense water formation and cascading in the Gulf of Thermaikos (North Aegean), from observations and modelling. Continental Shelf Research, 25, 2366-2386. https://doi.org/10.1016/j.csr.2005.08.014

Estournel C., Durrieu de Madron X., Marsaleix P., Auclair F., Julliand C. and R. Vehil (2003). Observation and modeling of the winter coastal oceanic circulation in the Gulf of Lion under wind conditions influenced by the continental orography (FETCH experiment). Journal of geophysical research, 108 (C3). https://doi.org/10.1029/2001JC000825

Estournel C., Broche P., Marsaleix P., Devenon J.L., Auclair F. and Vehil R. (2001). The Rhone River Plume in Unsteady Conditions: Numerical and Experimental Results. Estuarine, Coastal and Shelf Science, 53, 25-38. https://doi.org/10.1006/ecss.2000.0685

Ferrarin C., Bergamasco A., Umgiesser G., Cucco A. (2013). Hydrodynamics and spatial zonation of the Capo Peloro coastal system (Sicily) through 3-D numerical modelling. Journal of Marine Systems, 1-49. doi:doi:10.1016/j.jmarsys.2013.02.005

Geyer W. R. (1997). Influence of Wind on Dynamics and Flushing of Shallow Estuaries. Estuarine, Coastal and Shelf Science, 44(6), 713-722. https://doi.org/10.1006/ecss.1996.0140

Geyer W. R., Morris J. T., Prahl F., G.; Jay D. A. (2000). Interaction entre les processus physiques et la structure de l'écosystème; Une approche comparative (eurekamag.com). In: Hobbie, J.E. (Ed.), Estuarine Science: a Synthetic Approach to Research and Practice. Island Press, Washington, DC,, 177–206.

Guèdjè K. F., Houeto A. V.V., Houngninou B. E., Fink H. A. and Knippertz P. (2019). Climatology of coastal wind regimes in Benin. Meteorol. Z. (Contrib. Atm. Sci.), 28(1), 23–39. http://dx.doi.org/10.1127/metz/2019/0930

Guragai B., Hashimoto T., Oguma K., Takizawa S. (2018). Data logger-based measurement of household water consumption and micro-component analysis of an intermittent water supply system. Journal of Cleaner Production, 197(1), 1159-1168. https://doi.org/10.1016/j.jclepro.2018.06.198

Herbert G., Ayoub N., Marsaleix P. and Lyard F. (2011). Signature de la variabilité de la circulation côtière dans les données altimétriques dans le sud du golfe de Gascogne au cours de l'hiver et de l'automne 2004. Journal des systèmes marins, 88 (2), 139-158. https://doi.org/10.1016/j.jmarsys.2011.03.004

Hu Z.Y., Doglioli A. M., Petrenko A. A., Marsaleix P., Dekeyser I. (2009). Numerical simulations of eddies in the Gulf of Lion. Ocean Modelling, Elsevier, 28 (4), 203-208. https://doi.org/10.1016/j.ocemod.2009.02.004

Jouon A., Douillet P., Ouillon S., Fraunie P. (2006). Calculations of hydrodynamic time parameters in a semi-opened coastal zone using a 3D hydrodynamic model. Continental Shelf Research 26, 1395–1415. doi:10.1016/j.csr.2005.11.014

Lerczak A. J., Geyer W. R. (2006). Mechanisms Driving the Time-Dependent Salt Flux in a Partially Stratified Estuary. Journal of Physical Oceanography, 36, 2296-2311. https://doi.org/10.1175/JPO2959.1

Du J., Park K., Shen J., Zhang Y. J., Yu X., Ye F., Wang Z., Rabalais N. N. (2019). A hydrodynamic model for Galveston Bay and the shelf in the northern Gulf of Mexico. Ocean Science, 951–966. https://doi.org/10.5194/os-15-951-2019

Kjerfve, B. (1994) Coastal Lagoons. In: Kjerfve, B., Ed., Coastal Lagoon Processes, Elsevier Oceanographic Series, Amsterdam, 1-8.

Koutitonsky V. G., T. Guyondet, A. ST-Hilaire, S. C. Courtenay, A. Bohgen (2004). Water Renewal Estimates for Aquaculture Developments in the Richibucto Estuary, Canada. Estuaries, Vol. 27, No. 5, p. 839–850

Lacy J. R., Stacey M. T., Burau J. R., Monismith S. G. (2003), Interaction of lateral baroclinic forcing and turbulence in an estuary, *J. Geophys. Res.*, 108, 3089, C3. https://doi.org/10.1029/2002JC001392

Lalèyè, P., Philippart J.C., Poncin, P. (1995). Reproductive biology of two species of Chrysichthys (Siluriformes, Bagridae) from Lake Nokoué and the PortoNovo Lagoon in Benin. Journal of African Zoology, 109(3), 213-224.

Lalèyè P., Niyonkuru C., Moreau J., Teugels G.G. (2003). Spatial and seasonal distribution of the ichthyofauna of lake Nokoué, Benin, West Africa. African Journal of Aquatic Science, 28(2), 151–161. https://doi.org/10.2989/16085910309503779

Lalèyè P., Villanueva M.C., Entsua-Mensah M., Moreau J. (2007). A review of the aquatic living resources in Gulf of Guinea lagoons, with particular emphasis on fisheries management issues. J. Afrotrop. Zool. Special issue : 123-136. Belgium.

Lane R. R., Madden C. J., Day J.W., Solet D. J. (2011). Hydrologic and nutrient dynamics of a coastal bay and wetland receiving discharge from the Atchafalaya River. Hydrobiologia 658, 55–66. https://doi.org/10.1007/s10750-010-0468-4

Liu W.-C., Chen W-B., Hsu M-H.(2010). Using a three-dimensional particle-tracking model to estimate the residence time and age of water in a tidal estuary. Computers & Geosciences, 37, 1148–1161. https://doi.org/10.1016/j.cageo.2010.07.007

Loisel H., Vantrepotte V., Ouillon S., Ngoc D.D., Marine H., Tran V., Mériaux X., Dessailly D., Jamet C., Duhaut T., Nguyen H.H., Van Nguyen T. (2017). Assessment and analysis of the chlorophyll-a concentration variability over the Vietnamese coastal waters from the MERIS ocean color sensor (2002–2012). Remote Sensing of Environment, 190, 217–232. http://dx.doi.org/10.1016/j.rse.2016.12.016

Lovato T., Androsov A., Romanenkov D., Rubino A. (2010). The tidal and wind induced hydrodynamics of the composite system Adriatic Sea/Lagoon of Venice. Continental Shelf Research, 692-706. https://doi.org/10.1016/j.csr.2010.01.005

Maier-Reimier. (1977). Residual circulation in the North Sea due to the M 2 tide and mean annual wind stress. Deutsche Hydrographische Zeitschrift., 69-80. https://doi.org/10.1007/BF02227045

Mama D., Deluchat V., Bowen J., Chouti W., Yao B., Gnon B., Baudu M. (2011). Caractérisation d'un Système Lagunaire en Zone Tropicale: Cas du lac Nokoué(Bénin). European Journal of Scientific Research, 56(4), 516-528.

Maraldi C., Chanut J., Levier B., Ayoub N., De Mey P., Reffray G., Lyard F., Cailleau S., Drévillon M., Fanjul E. A., Sotillo M. G., Marsaleix P. (2013). NEMO on the shelf: assessment of the Iberia–Biscay–Ireland configuration. Ocean Science, 9, 745–771. https://doi.org/10.5194/os-9-745-2013

Marine. J. H., Diaz F., Estournel C., Marsaleix P., Ulses C. (2013). Impact of atmospheric and oceanic interannual variability on the Northwestern Mediterranean Sea pelagic planktonic ecosystem and associated carbon cycle. Journal Geophysical Research : Ocean, 118, 5792–5813. https://doi.org/10.1002/jgrc.20405

Marine. J. H., and Somot S. (2008). Relevance of ERA40 dynamical downscaling for modeling deep convection in the Mediterranean Sea. Geophysical Research Letters, 35 (L04607). https://doi.org/10.1029/2007GL032442

Marsaleix P., Auclair F., Estournel C. (2006). Considerations on Open Boundary Conditions for Regional and Coastal Ocean Models. Journal of Atmospheric and Oceanic Technoloy, 23, 1604-1613. https://doi.org/10.1175/JTECH1930.1

Marsaleix P., Auclair F., Floor J. W., Marine H. J., Estournel C., Pairaud I., Ulses C. (2008). Energy conservation issues in sigma-coordinate free-surface ocean models. Ocean Modelling, 20, 61–89. https://doi.org/10.1016/j.ocemod.2007.07.005

McIntosh P. (1990). Oceanographic data interpolation: Objective analysis and splines. Journal of Geophysical Research, 95, 13529–13541. https://doi.org/10.1029/JC095iC08p13529

Michaud H., Marsaleix P., Leredde Y., Estournel C., Bourrin F., Lyard F., Mayet C., Ardhuin F. (2012). Three-dimensional modelling of wave-induced current from the surf zone to the inner shelf. Ocean Science, 8, 657–681. https://doi.org/10.5194/os-8-657-2012

Mohanty P. K. & Panda B. U. S. (2009). : Circulation and mixing processes in Chilika lagoon. Indian Journal of Marine Sciences, 205-214. http://nopr.niscpr.res.in/handle/123456789/4671

Monsen N. E., Cloern E. J., Lucas V. L., Monismith G. S. (2002). A comment on the use of flushing time, residence time, and age as transport time scale. American Society of Limnology and Oceanography, 47 (5), 1545–1553. doi: https://doi.org/10.4319/lo.2002.47.5.1545

Morales M., Aquije J., Carvalho L., Mejía A. (2020). Hydrodynamic Modelling of a Coastal Lagoon in México. Revista de Investigación de Física. https://doi.org/10.15381/rif.v23i3.20301

Morel Y., Chaigneau A., Okpeitcha O. V., Stieglitz T., Rétif F., Duhaut T., Sohou Z. (2022). Terrestrial or oceanic forcing? Water level variations in coastal lagoons. Advances in Water Resources, 169 (104309). https://doi.org/10.1016/j.advwatres.2022.104309

Mudge M. S., Glacé D. J., Newton A.(2008). Residence times in a hypersaline lagoon: Using salinity as a tracer. Estuarine, Coastal and Shelf Science, 77, 278-284. https://doi.org/10.1016/j.ecss.2007.09.032

Newton A., Brito A.C., Icely J.D., Derolez V., Clara I., Angus S., Schernewski G., Inacio, M., Lillebø, A.I., Sousa, A.I., Béjaoui B., Solidoro C., Tosic M., Canedo-Argüelles M., Yamamuro M., Reizopoulou S., Tseng H.-C., Canu D., Roselli L., Maanan M., Cristina S., Ruiz-Fernandez, A.C., de Lima R.F., Kjerfve, B., Rubio-Cisneros, N., Pérez-Ruzafa A., Marcos C., Pastres R., Pranovi F., Snoussi M., Turpie J., Tuchkovenko Y., Dyack B. (2018). Assessing, quantifying and valuing the ecosystem services of coastal lagoons. Journal for Nature Conservation, 50-65. https://doi.org/10.1016/j.jnc.2018.02.009

Niyonkuru C. & Lalèyè P.A. (2010). Impact of acadja fisheries on fish assemblages in Lake Nokoué, Benin, West Africa. Knowledge and Management of Aquatic Ecosystems,399, 05 https://doi.org/10.1051/kmae/2010033.

O'Callaghan J. and C. Stevens. (2011). Wind Stresses on Estuaries. Estuarine and Coastal Science, 151-166. https://doi.org/10.1016/B978-0-12-374711-2.00211-4

O'Callaghan J., Pattiaratchi C., Hamilton D. (2007). The response of circulation and salinity in a micro-tidal estuary to sub-tidal oscillations in coastal sea surface elevation. Continental Shelf Research , 1947-1965. https://doi.org/10.1016/j.csr.2007.04.004

Ogutu-Ohwayo R., Hecky E. R., Cohen S. A., Kaufman L. (1997). Human Impacts on the African Great Lakes. Environmental Biology of Fishes, 50(2), 117-131. http://dx.doi.org/10.1023/A:1007320932349

Okpeitcha V., Chaigneau A., Morel Y., Stieglitz T., Pomalegni Y., Sohou Z., Mama D. (2022). Seasonal and interannual variability of salinity in a large West-African lagoon (Nokoué Lagoon, Benin). Estuarine, Coastal and Shelf Science, 264(107689),1-10. https://doi.org/10.1016/j.ecss.2021.107689

Okpeitcha V., Chaigneau A., Morel Y., Duhaut T., Marsaleix P., Rétif F., Honfo J., Stieglitz T., Sintondji O. L., Sohou Z., Mama D. (2024). Modeling seasonal salinity variations in a large West African lagoon (Nokoué, Benin): Major drivers and mechanisms. Regional Studies in Marine Science 69 (2024) 103330. https://doi.org/10.1016/j.rsma.2023.103330

Onguéné R.. Modélisation multi-échelle de la circulation océanique en Afrique centrale, de la plaine abyssale à l'estuaire du Cameroun. Océanographie. Université Paul Sabatier - Toulouse III, 2015. Français. ffNNT : 2015TOU30393ff. fftel-03657048ff

Pairaud I. L., Lyard F., Auclair F., Letellier T., Marsaleix P. (2008). Dynamics of the semi-diurnal and quarter-diurnal internal tides in the Bay of Biscay. Part 1: Barotropic tides. Continental Shelf Research, 28, 1294– 1315. https://doi.org/10.1016/j.csr.2008.03.004

Panda U.S., Mahanty M. M., Rao R. V., Patra S. and Mishra P. (2015). Hydrodynamics and water quality in Chilika Lagoon-A modelling approach. Procedia Engineering, 639-646. https://doi.org/10.1016/j.proeng.2015.08.337

Peng C., Wang A., Wu J., Lin Y., Chen J., Chen N. (2021). An assessment of residence and influence times in Xiamen Bay, China. Estuarine, Coastal and Shelf Science, 262(107595). https://doi.org/10.1016/j.ecss.2021.107595

Pérez-Ruzafa A., Marcos C., Pérez-Ruzafa I. M. & Pérez-Marcos M. (2011). Coastal lagoons: "transitional ecosystems" between transitional and coastal waters. Journal of Coastal Conservation, 15(3), 369-392 (24 pages). https://doi.org/10.1016/j.ecss.2007.04.030

Pérez-Ruzafa A., Pérez-Ruzafa I. M., Newton A., Marcos C. (2019). Coastal Lagoons: Environmental Variability, Ecosystem Complexity, and Goods and Services Uniformity. Elsevier Coasts and Estuaries, 253-276. https://doi.org/10.1016/B978-0-12-814003-1.00015-0

Pritchard D. W. (1952). Salinity distribution and circulation in the Chesapeake Bay estuarine system. Journal of Marine Research, 106–123.

Robinson I. S. (1981). Tidal vorticity and residual circulation. Deep-Sea Researc, 28A(3), 195-212. https://doi.org/10.1016/0198-0149(81)90062-5

Rodhe H. (1992). Modeling Biogeochemical Cycles. Academic Press, pp. 55–71.

Sale P.F., Feary D.A., Burt J.A. (2011). The Growing Need for Sustainable Ecological Management of Marine Communities of the Persian Gulf. *AMBIO* **40**, 4–17. https://doi.org/10.1007/s13280-010-0092-6

Sassi M. G. and Hoitink A. J. F. (2013). River flow controls on tides and tide-mean water level profiles in a tidal freshwater river. Journal Of Geophysical Research: Oceans, 118, 4139–4151. https://doi.org/10.1002/jgrc.20297

Seyfried L., Marsaleix P., Richard E., and Estournel C. (2017). Modelling deep-water formation in the north-west Mediterranean Sea with a new air–sea coupled model: sensitivity to turbulent flux parameterizations. Ocean Sci., 13, pp 1093–1112. https://doi.org/10.5194/os-13-1093-2017

Swift S.A. and Bower A.S., (2013). Formation and circulation of dense water in the Persian/Arabian Gulf. Journal of Geophysical Research, 108(C1)(3004,). https://doi.org/10.1029/2002JC001360

Sylaios G. K., Tsihrintzis V. A., Akratos C. and Haralambidou K. (2006). Quantification of water, salt and nutrient exchange processes at the mouth of a mediterranean coastal lagoon. Environmental Monitoring and Assessment, 275-301. https://doi.org/10.1007/s10661-005-9026-3

Sylaios G., Tsihrintzis V.A., Akratos C., Tsikliras A., Haralambidou K. (2003). Residual currents and fluxes through the mouth of Vassova coastal lagoon. Mediterranean Marine Science, 39-52. https://doi.org/10.12681/mms.227

Takeoka H. (1984). Fundamental concepts of exchange and transport time scales in a coastal sea. Contmental Shelf Research, 3 (3), 311-326. https://doi.org/10.1016/0278-4343(84)90014-1

Texier H., Colleuil B., Profizi J-P., Dossou C. (1980). Le lac Nokoué, environnement du domaine margino-littoral sud-béninois : bathymétrie, lithofaciès, salinité, mollusque et peuplements végétaux. Bull. Inst. Geol. Bassin Aquitaine; ISSN 0524-0832; Fra(28), pp. 115-142.

Torres-Bejarano F.M., Torregroza-Espinosa A.C., Martinez-Mera E, Castañeda-Valbuena D., Tejera-Gonzalez D. (2020). Hydrodynamics and water quality assessment of a coastal lagoon using environmental fluid dynamics code explorer modeling system. Global Journal of Environmental Science and Management, 289-308. https://doi.org/10.22034/gjesm.2020.03.02

Nguyen-Duy T., Ayoub K. N., Marsaleix P., Toublanc F., De Mey-Frémaux P., Piton V., Marine H., Duhaut T., Tran C. M., Ngo-Duc T. (2021). Variability of the Red River Plume in the Gulf of Tonkin as Revealed by Numerical Modeling and Clustering Analysis. Frontiers in Marine Science , 8:772139. https://doi.org/10.3389/fmars.2021.772139

Ulses C., Estournel C., Bonnin J., Durrieu de Madron X., Marsaleix P. (2008). Impact of storms and dense water cascading on shelf-slope exchanges Impact of storms and dense water cascading on shelf-slope exchanges. Journal of Geophysical Research, 113 (C02010). https://doi.org/10.1029/2006JC003795

Umgiesser, G., C. Ferrarin, A. Cucco, F. De Pascalis, D. Bellafiore, M. Ghezzo, and M. Bajo (2014). Comparative hydrodynamics of 10 Mediterranean lagoons by means of numerical modeling, J. Geophys. Res. Oceans, 119, 2212–2226, doi:10.1002/2013JC009512.

Villanueva M.C., Lalèyè P., Albaret J.J., Laë R., Morais L. T., Moreau J. (2006). Comparative analysis of trophic structure and interactions of two tropical lagoons. Ecological modelling, 197, 461–477.

Welcomme, R.L. (1972), An evaluation of the acadja method of fishing as practised in the coastal lagoons of Dahomey (West Africa). Journal of Fish Biology, 4: 39-55. https://doi.org/10.1111/j.1095-8649.1972.tb05651.x

Wilson G.V., Rigby J.R., Ursic M., Dabney S.M., (2016). Soil pipe flow tracer experiments: 1. Connectivity and transport characteristics. Hydrological Processes, 30, 1265–1279. https://doi.org/10.1002/hyp.10713

Wong A. P. S., Johnson C.G., Owens W. B. (2003). Delayed-Mode Calibration of Autonomous CTD Profiling Float Salinity Data by u–S Climatology. Journal of atmospheric and Oceanic Technology, 20, 308-318. https://doi.org/10.1175/1520-0426(2003)020%3C0308:DMCOAC%3E2.0.CO;2

Yehouenou E.A.P., Adamou R., Azehoun P.J., Edorh P.A. and Ahoyo T. (2013, May). Monitoring of Heavy Metals in the complex "Nokoué lake - Cotonou and Porto-Novo lagoon " ecosystem during three years in the Republic of Benin. Research Journal of Chemical Sciences, 3(5).

Zandagba J., Adandedji M. F., Mama D., Chabi A., Afouda A. (2016). Assessment of the Physico-Chemical Pollution of a Water Body in a Perspective of Integrated Water Resource Management: Case Study of Nokoué Lake. Journal of Environmental Protection, 7, 656-669. http://dx.doi.org/10.4236/jep.2016.75059

Zimmerman J. T. F. (1988). Estuarine residence times. (H. o. In B. Kjerfve [ed.], Éd.) Consulté le 10 23, 2022. https://doi.org/10.1201/9781351073257